CHALMERS

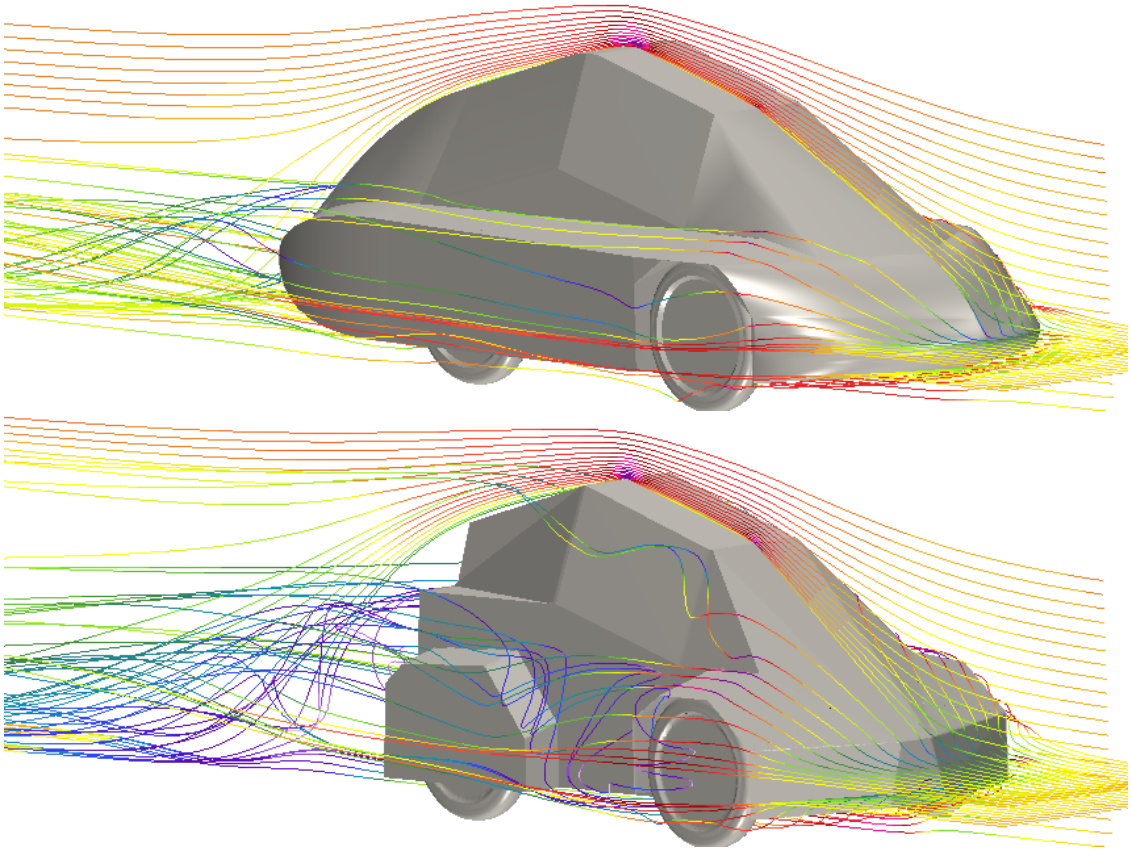

Smarter Aerodynamics

Aerodynamic improvement of Chalmers' Shell Eco-marathon car Smarter

Bachelor's thesis in Applied Mechanics

FILIP LJUNGSTRÖM
MARTIN OTTOSSON
MOHAMMED SAEED
EMMA SUNDELL
IDA TRANGSRUD
DAVID WINQVIST

Department of Applied Mechanics
Division of Vehicle Engineering and Autonomous Systems
CHALMERS UNIVERSITY OF TECHNOLOGY
Gothenburg, Sweden 2016

Bachelor's thesis 2016:07

Bachelor's project TMEX02-16-09

Smarter Aerodynamics

Aerodynamic improvement of Chalmers' Shell Eco-marathon car Smarter

Bachelor's project in Applied Mechanics

Filip Ljungström
Martin Ottosson
Mohammed Saeed
Emma Sundell
Ida Trangsrud
David Winqvist

Department of Applied Mechanics
Vehicle Engineering and Autonomous Systems
Chalmers University of Technology
Gothenburg, Sweden 2016

Smarter Aerodynamics
Aerodynamic improvement of Chalmers' Eco-marathon car Smarter
Bachelor's project in Applied Mechanics
Filip Ljungström
Martin Ottosson
Mohammed Saeed
Emma Sundell
Ida Trangsrud
David Winqvist

© Filip Ljungström Martin Ottosson Mohammed Saeed Emma Sundell Ida Trangsrud David Winqvist, 2016

Bachelor's thesis 2016:07
ISSN 1654:4676
Department of Applied Mechanics
Division of Vehicle Engineering and Autonomous Systems
Chalmers University of Technology
SE-412 96 Gothenburg
Sweden
Telephone: + 46 (0)31-772 1000

Cover: Streamlines of the flow around the final design (above) and original design (below).

Department of Applied Mechanics
Gothenburg, Sweden 2016

Abstract

Students at Chalmers have participated in the UrbanConcept class in the Shell Eco-marathon competition since 2009. The aim of the competition is to build and drive a car as far as possible with an amount of energy equivalent to 1 litre of petrol. Chalmers' current car is called Smarter and has been manufactured at the university campus, meaning that there were some limitations regarding manufacturing possibilities. Therefore, a simple body design was chosen, consisting of flat plates made out of plastic material. This design was assumed to result in poor aerodynamic properties, which gave rise to this Bachelor's thesis.

The purpose of this thesis was to improve the aerodynamic properties of the car and thereby lower the air drag, without compromising the possibility of manufacturing it at Chalmers. This has been done through examining the properties of the original design with flow simulations in STAR-CCM+ and in a following design process improve the design from an aerodynamic perspective. Several designs were presented during the design process and the best designs were selected and presented in a final design.

The final design has a drag coefficient of about 34% of the coefficient for the original design, which will contribute to a better fuel efficiency.

Sammanfattning

Chalmersstudenter har sedan 2009 medverkat i UrbanConcept-klassen i tävlingen Shell Eco-marathon. Målet i tävlingen är att bygga och sedan köra en bil så långt som möjligt med mängden energi motsvarande en liter bensin. Chalmers nuvarande bil kallas för Smarter och har tillverkats i högskolans lokaler vilket har inneburit vissa begränsningar i tillverkningsteknik. Detta har gjort att man valt en simpel karossdesign bestående av plana plattor i plastmaterial. Denna design antogs medföra dåliga aerodynamiska egenskaper, vilket gav upphov till detta kandidatarbete.

Syftet med arbetet var att förbättra bilens aerodynamiska egenskaper och därmed sänka dess luftmotstånd, utan att äventyra möjligheten att kunna bygga den på Chalmers. Detta har gjorts genom att utvärdera bilens ursprungliga aerodynamik med hjälp av strömningssimuleringar i STAR-CCM+, för att sedan i en designprocess förbättra bilens design ur ett aerodynamiskt perspektiv. Flera designer presenterades under designprocessen och de bästa valdes ut och presenterades i en slutgiltig design.

Den slutliga designen har en luftmotståndskoefficient på ca 34% av den ursprungliga, vilket kommer att bidra till en bättre bränsleeffektivitet.

Keywords: CFD, drag force, drag coefficient, Shell Eco-marathon, STAR-CCM+, vehicle aerodynamics

Preface

This report presents the work and results of a Bachelor's thesis done during the period 2016-01-21 to 2016-05-17 at the Department of Applied Mechanics at Chalmers University of technology, Gothenburg, Sweden. The purpose of the thesis was to improve the aerodynamic properties of the car Smarter, which is Chalmers' contribution to the UrbanConcept class in the Shell Eco-marathon competition. Analysis of the properties was made through flow simulations in the CFD software STAR-CCM+.

Acknowledgements

First of all we would like to thank our supervisor, Ph.D. student Emil Ljungskog, who came up with the idea for this Bachelor's thesis. He has been a great help by always being available, responding to questions and giving tips when problems have occurred. We would also like to thank him for the study visit at Volvo's wind tunnel and last but not least for the outstanding fudge he brought to one of our meetings.

Secondly, we would like to thank our examiner, Associate Professor Simone Sebben, for feedback, tips and useful presentations of CFD analysis.

We would also like to show our appreciation for the mechanical engineering program at Chalmers for providing us with the computer cluster used for simulations.

At last, thanks to Professor Sven B Andersson and the Smarter team for the information about Smarter and Shell Eco-marathon.

The authors, Gothenburg, May 2016

Contents

Nomenclature **xi**

1 Introduction **1**
1.1 Purpose . . . 1
1.2 Problem Statement . . . 1
1.3 Delimitations . . . 2
1.4 Background . . . 2
1.4.1 Shell Eco-marathon . . . 2
1.4.2 Shell Eco-marathon Regulations . . . 3
1.4.3 Smarter 2015 . . . 4

2 Theory **7**
2.1 Foundations of Fluid Dynamics . . . 7
2.1.1 Incompressible Flow . . . 7
2.1.2 Reynolds Number . . . 7
2.1.3 Reynolds Transport Theorem . . . 8
2.1.4 Navier-Stokes Equations . . . 9
2.1.5 Laminar and Turbulent Flow . . . 9
2.1.6 Reynolds-averaged Navier–Stokes Equations (RANS-equations) 10
2.1.7 Turbulence Modelling with Realizable k-epsilon . . . 11
2.1.8 Separation of Flow . . . 11
2.1.9 The Boundary Layer Equations . . . 13
2.1.10 Drag and Lift Coefficients . . . 14
2.1.11 Pressure Coefficient . . . 14
2.1.12 Total Pressure Coefficient . . . 15
2.2 Vehicle Aerodynamics . . . 15
2.2.1 Drag Force . . . 15
2.2.2 Lift Force . . . 16
2.2.3 Example of Drag Coefficient Values . . . 16
2.3 Other Relevant Vehicle Dynamics . . . 17
2.4 The Finite Volume Method . . . 17

3 Methods **19**
3.1 Pre-Processing . . . 20
3.1.1 Clean-up Process . . . 20
3.1.2 Categorizing Surfaces . . . 21

3.1.3 Meshing . . . 21
3.2 Processing . . . 22
3.2.1 Boundary Conditions . . . 23
3.2.2 Physical Model . . . 23
3.3 Post-Processing . . . 23
3.4 Analysis and Redesign . . . 24
3.5 Mesh Dependency Study and Computational Resources Determination 24

4 Original Design 27

5 Design Process 31
5.1 Standard 1 . . . 31
5.2 Front Modifications . . . 32
5.2.1 Short Nose Shaped Front . . . 33
5.2.2 Long Nose Shaped Front . . . 34
5.2.3 Rounded Front Wheel Fenders . . . 34
5.2.4 Rounded A-pillars . . . 35
5.2.5 Sum up of Front Modifications . . . 36
5.3 Standard 2 . . . 38
5.4 Rear Modifications . . . 39
5.4.1 Edgy Boat Tail . . . 40
5.4.2 Rounded Boat Tail . . . 41
5.4.3 Rounded Top and Reduced Rear Wheels Opening . . . 42
5.4.4 Cavity . . . 43
5.4.5 Sum up of Rear Modifications . . . 45
5.5 Other Modifications . . . 46

6 Final Design 49
6.1 Geometry . . . 49
6.2 Analysis . . . 51

7 Discussion 57
7.1 Comments on Methods . . . 57
7.2 Comments on Results . . . 58
7.2.1 Final Design . . . 58
7.2.2 Other Configurations . . . 60
7.2.3 Further Improvements . . . 60

8 Conclusion 63

Bibliography 66

Nomenclature

$\overline{(\cdot)}'$	Fluctuating component
$\overline{(\cdot)}$	Time averaged component
β	The quantity of a property B per unit mass: $\frac{\mathrm{d}B}{\mathrm{d}m}$
δ_{ij}	Kronecker delta
ϵ	Dissipation rate of the turbulent kinetic energy
η	Efficiency of the powertrain
$\mathbf{n}$	Normal unit vector
$\mathbf{V_r}$	Velocity vector relative to the velocity of a control volume
$\mathbf{V}$	Velocity vector
μ	Dynamic viscosity
ν	Kinematic viscosity
ν_t	Turbulent viscosity
ρ	Density of the fluid in a flow
τ_w	Wall shear stress
A	Characteristic area
B	A scalar or vector property of a fluid
C_D	Drag coefficient
C_L	Lift coefficient
C_p	Pressure coefficient
C_μ	Constant used in k-ϵ-model
$C_{p,tot}$	Total pressure coefficient
E	Energy content in the fuel
F_D	Drag force
F_L	Lift force
F_R	Rolling resistance
g	Gravitational acceleration
k	Turbulent kinetic energy
L	Characteristic length
p	Pressure
p_∞	Free stream pressure
p_{tot}	Total pressure
s	Distance
U	Free stream velocity
u	Flow velocity component in the x-direction
u^*	Friction velocity
V	Characteristic velocity
v	Flow velocity component in the y-direction

W	Work
w	Flow velocity component in the z-direction
y^+	Dimensionless coordinate along a boundary layer
CAD	Computer aided design
CFD	Computational fluid dynamics
CS	Control surface
CV	Control volume
F	Force
FVM	Finite volume method
PID	Property ID
Re	Reynolds number

1
Introduction

Shell Eco-marathon is a competition in which students from universities all over the world compete in building the most energy efficient car. The task is to get the car to run as far as possible with an amount of energy equivalent to 1 litre of petrol. Chalmers students have been participating in the UrbanConcept class of the competition since 2009, in which the passenger comfort and practical designs are to be considered in addition to energy efficiency [1]. There have been several generations of Chalmers' car, named Smarter, during the years. Each year a new group of students from the university, from now on referred to as "the Smarter team", builds a new version of the car. The current design results from the performance being based on weight and simple manufacturing rather than aerodynamics, resulting in an edgy design. The potential of decreasing the air drag is therefore considered to be high, which is the focus of this project. Note that the students behind this project, focusing on the aerodynamics, are not part of the Smarter team.

1.1 Purpose

The general purpose of this Bachelor's thesis is to present a suggestion of a new design for the body of Chalmers' Shell Eco-marathon car, Smarter. The new suggested design should have a reduced air drag of at least 10% without having substantial changes in lift force. The Smarter team's possibility to implement the new design with regard to manufacturing resources should also be taken into consideration when presenting a new body design.

1.2 Problem Statement

To be able to achieve the purpose of this Bachelor's thesis some questions need to be answered. If the aerodynamics of Smarter are to be improved the aerodynamics of the current design will need to be evaluated. The first question will therefore be: which are the aerodynamic flaws of the current design? If the flaws can be identified the next step will be to eliminate these. The next question will therefore be: how could the biggest problem areas be improved while still taking into account the restrictions of the manufacturing process and the regulations of the competition?

The framing of questions can be summarized as:

- Which are the aerodynamic flaws of the current design?

- How could the biggest problem areas be improved while still taking the existing restrictions into account?

1.3 Delimitations

This Bachelor's thesis only intended to improve the aerodynamics Smarter. Therefore no changes have been done on other parts of Smarter, such as chassis or the wheel suspension. The thesis is only based on computer simulations and therefore no resources have been spent on manufacturing a physical model of Smarter. This also means that no physical tests have been done on the model, in for example a wind tunnel.

Another limitation was the resource of computational power. When using computational fluid dynamics to calculate flows a great number of equations need to be solved which requires computational power. In this project a workstation with 20 cores was used for some calculations but mainly for pre- and post-processing. For processing a computer cluster was used.

A part of the purpose of this project is that the Smarter team must be able to manufacture the final design. The restriction that exists is basically that they must build the body in their workshop, without help from a third party. This means that the body mainly must consist of flat plates and parts that are bent in maximum one direction. To create more complex geometries e.g. styrofoam can be used.

1.4 Background

This section presents the setup of the competition Shell Eco-Marathon and its regulations. A brief explanation of Chalmers' car Smarter is also included.

1.4.1 Shell Eco-marathon

As previously mentioned, the purpose of Shell Eco-marathon is to let university students compete in building the most energy efficient car. The concept of the competition is to get the cars to run as far as possible with an amount of energy equivalent to 1 litre of petrol. There are three events in total which are run separately in Europe, Asia and America. The competition is split into two classes: Prototype and UrbanConcept. The prototype class is only focusing on energy efficiency. The UrbanConcept class is encouraging more practical designs, such as passenger comfort and luggage space, in addition to energy efficiency. The competition is also divided into different categories with respect to energy sources. These categories consist of different combustion engines, electric motors and hybrids.

The competition lasts for several days and the participants get to make as many attempts as possible to get their car to travel the furthest. The cars run a fixed

number of laps around a circuit and after each attempt the energy efficiency is calculated. Finally a winner for each class is presented. There are also some off-track awards regarding safety, teamwork and design [1].

1.4.2 Shell Eco-marathon Regulations

Aerodynamic changes on the car's body and chassis are limited by the regulations of the competition. The outer dimensions are limited by the following measures, some of them can be seen in figure 1.1.

- Height between 100 and 130 cm
- Total body width between 120 and 130 cm
- Length between 220 and 350 cm
- Track width at least 100 cm for front axle and 80 cm for rear axle
- Wheelbase, length between front and rear axle, must be at least 120 cm
- Ground clearance at least 10 cm
- Maximum weight excluding the driver is 225 kg
- The drivers compartment must have a height of at least 88 cm and a width (at the drivers shoulders) of at least 70 cm [2]

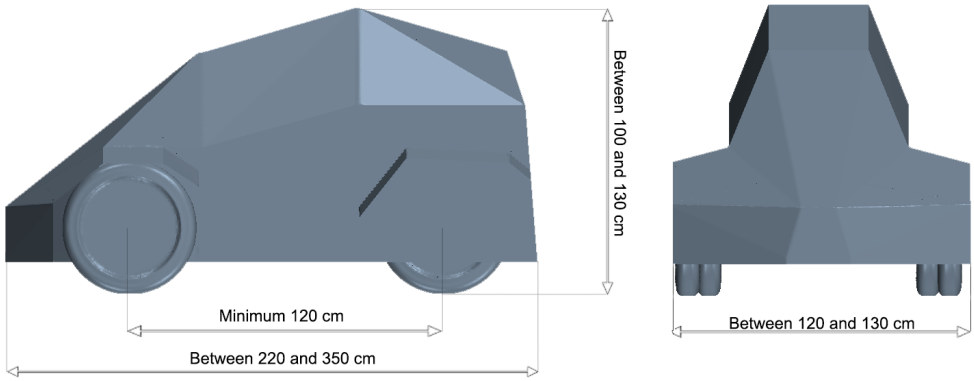

Figure 1.1: *Some dimensions set by Shell Eco-marathon regulations. Note that these are not the actual dimensions of Smarter.*

In addition to the outer dimensions there are several other rules that are relevant for an aerodynamic improvement and will be needed to be taken into account.

- Aerodynamic appendages, which adjust or are prone to changing shape due to wind whilst the vehicle is in motion, are forbidden.
- Vehicle body must not include any external appendages that might be dangerous to other team members, e.g. pointed part of the vehicle body. Any sharp points must have a radius of 5 cm or greater, alternatively they should be made of foam or similar deformable material.
- Vehicle body panels must be rigid with an appropriate stiffness not to be prone to changing shape due to wind.

- The vehicle must be fully covered.
- The driver must have access to a direct arc of visibility ahead and to 90° on each side of the longitudinal axis of the vehicle.
- The vehicle must be equipped with a sufficiently large opening for the cockpit. The door must have a dimension of at least 50x80 cm.
- There must be a luggage space with dimensions 500 x 400 x 200 (L x H x W).
- The turning radius must be at least 6 m [2].

1.4.3 Smarter 2015

The body of Smarter is designed for good strength and stability using a tubular space frame and a single seater cockpit design. The Smarter team focused on weight reduction and simple manufacturing rather than reducing drag, hence the edgy design. The design of Smarter can be seen in figure 1.2, and the dimensions are specified in figure 1.3. This design can be considered to have a large potential for improvement with respect to aerodynamics, thus maximizing fuel efficiency by lowering the drag. The car runs on ethanol making it the first Chalmers EcoSmarter to be participating in the Ethanol category [3].

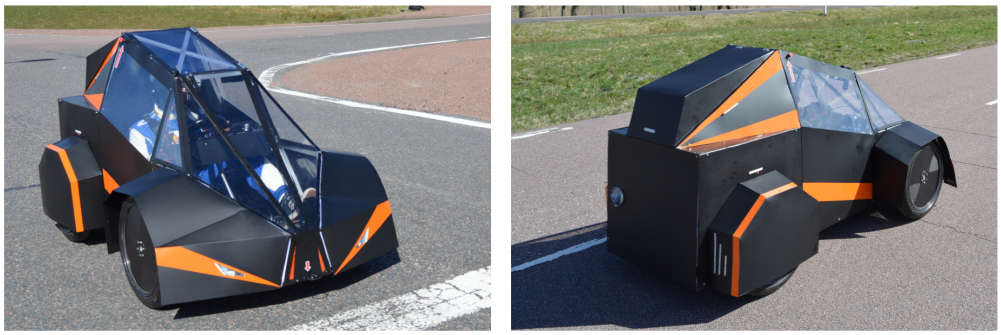

Figure 1.2: *Smarter 2015.*

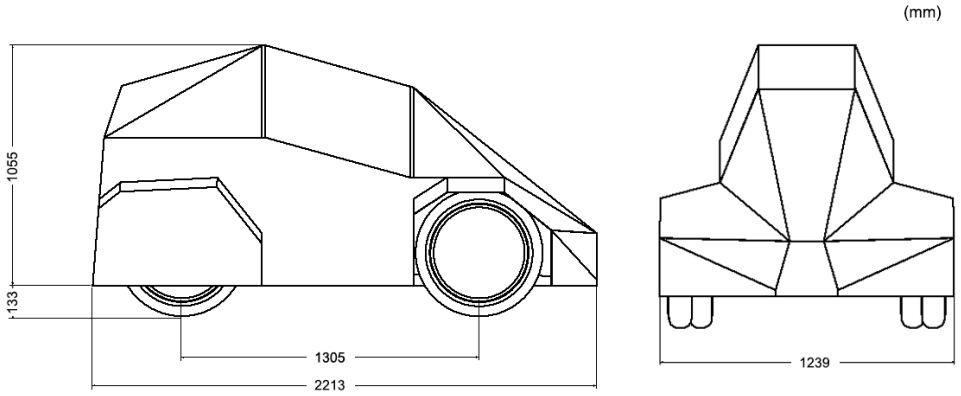

Figure 1.3: *Dimensions of Smarter 2015.*

Car specifications

- Engine: 35 cc, 4-stroke, 2 valve, air-cooled
- DC-Motor: Maxon Motor RE65-250W
- Chassis: tubular space frame with aluminium tubes
- Innovations: series hybrid, free rolling
- Energy Storage: supercapacitor
- Fuel: ethanol [3]

2

Theory

This chapter includes the most fundamental theory that this project is based on. It starts with presenting some foundations of fluid dynamics. Furthermore a more general description of different phenomena and applications for vehicle aerodynamics is explained. Finally a short explanation about the finite volume method are included, which is the method implemented in the computational fluid dynamics (CFD) software used in this project.

2.1 Foundations of Fluid Dynamics

In this section a brief introduction is given to understand the basics of fluid dynamics important for this project.

2.1.1 Incompressible Flow

Incompressible flow means that the density in the fluid is constant. This is an approximation that is considered valid when the velocity is around one third of the speed of sound or lower (for air, this means that incompressible flow is valid for velocities below 114 m/s at atmospheric pressure). For higher velocities the flow needs to be considered as compressible and changes in the density must be taken into account [4].

2.1.2 Reynolds Number

Reynolds number is a dimensionless parameter that is commonly used within fluid dynamics to determine specific characteristics and behaviours of a flow. Reynolds number is defined by

$$\mathrm{Re} = \frac{\rho V L}{\mu}, \tag{2.1}$$

where ρ is the fluid density and V is the characteristic velocity of the flow, typically the free stream velocity. Furthermore, L is the corresponding characteristic length, which can be for example the length of a body immersed in the fluid or the diameter of the pipe when considering flow in a duct. The remaining parameter μ is the dynamic viscosity of the fluid, which represents the ability to resist motion [4].

2.1.3 Reynolds Transport Theorem

The laws of mechanics, for example the law describing conservation of mass and Newton's second law, are written with respect to a system. This means that the laws should be applied to an arbitrary, fixed amount of mass. When studying the behaviour of a fluid it is more desirable to consider these laws for a specific region rather than a quantity of mass. Therefore, we want to convert the laws of mechanics to hold for a specific region instead for a fixed amount of mass. This conversion is done by the use of Reynolds transport theorem, which can be applied to all the basic laws of mechanics. The region that is considered is called the control volume (CV) and the boundaries to this volume is called control surface (CS). The general form of Reynolds transport theorem is formulated as

$$\frac{\mathrm{d}}{\mathrm{d}\,t}(B_{\text{syst}}) = \frac{\mathrm{d}}{\mathrm{d}\,t}\left(\int_{\text{CV}} \beta\rho \,\mathrm{d}\mathscr{V}\right) + \int_{\text{CS}} \beta\rho(\mathbf{V_r}\cdot\mathbf{n})\,\mathrm{d}A \tag{2.2}$$

where ρ is the fluid density, B represents any scalar or vector property of the fluid (mass, energy, momentum, etc.) and $\beta = \frac{\mathrm{d}B}{\mathrm{d}m}$. Moreover, $\mathbf{V_r}$ represents the velocity of the fluid relative to the velocity of the control volume and $\mathbf{n}$ the unit vector normal to the control surface. The first term in the right hand side in equation (2.2) describes the change of B within the control volume, while the second term represents the total amount of inflow and outflow of B over the control surface.

Often various simplifications can be done on the general form of Reynolds transport theorem given in equation (2.2). To begin with, if the control volume is fixed, that is neither moving nor deformable, the volume elements $\mathrm{d}\mathscr{V}$ do not vary with time. This means that the time derivative of the volume integral in equation (2.2) can be moved inside the integral. Furthermore, since the velocity of a fix control volume is zero, the relative velocity $\mathbf{V_r}$ is just assigned $\mathbf{V}$, which is the velocity of the fluid. Hence, in the case of fix control volume, Reynolds transport theorem can be written as

$$\frac{\mathrm{d}}{\mathrm{d}\,t}(B_{\text{syst}}) = \int_{\text{CV}} \frac{\partial}{\partial t}(\beta\rho)\,\mathrm{d}\mathscr{V} + \int_{\text{CS}} \beta\rho(\mathbf{V}\cdot\mathbf{n})\,\mathrm{d}A. \tag{2.3}$$

Furthermore, if the flow can be considered incompressible the density will not change with time and $\frac{\partial\rho}{\partial t} = 0$. On the other hand, if the flow within the control volume is assumed to be steady, which means that it is assumed to not vary with time, it holds that $\frac{\mathrm{d}}{\mathrm{d}t} = 0$ and the first term on the right hand side in Reynolds transport theorem cancels completely.

As two examples, we will consider Reynolds transport theorem letting the dummy variable B represent first mass, which corresponds to the law of conservation of mass, and then linear momentum, corresponding to Newton's second law. In the first case when B represents mass, we have that $B = m$ and $\beta = \mathrm{d}m/\mathrm{d}m = 1$. Equation (2.2) then becomes

$$\left(\frac{\mathrm{d}\,m}{\mathrm{d}\,t}\right)_{\text{syst}} = 0 = \frac{\mathrm{d}}{\mathrm{d}\,t}\left(\int_{\text{CV}} \rho \,\mathrm{d}\mathscr{V}\right) + \int_{\text{CS}} \rho(\mathbf{V_r}\cdot\mathbf{n})\,\mathrm{d}A. \tag{2.4}$$

When considering the correspondence to Newton's second law the dummy variable B represents the linear momentum $m\mathbf{V}$. That is, $\mathbf{B} = m\mathbf{V}$ and $\beta = \mathrm{d}\mathbf{B}/\mathrm{d}m = \mathbf{V}$. Inserting this into Reynolds transport theorem given in equation (2.2) gives

$$\frac{\mathrm{d}}{\mathrm{d}\,t}(m\mathbf{V})_{\text{syst}} = \sum \mathbf{F} = \frac{\mathrm{d}}{\mathrm{d}\,t}\left(\int_{\text{CV}} \mathbf{V}\rho \,\mathrm{d}\mathscr{V}\right) + \int_{\text{CS}} \mathbf{V}\rho(\mathbf{V_r}\cdot\mathbf{n})\,\mathrm{d}A. \tag{2.5}$$

This equation represents, as indicated by $\sum \mathbf{F}$, the vector sum of all forces on the control volume and the control surface. Furthermore, since the fluid velocity $\mathbf{V}$ is a vector, the last equation becomes a vector relation with three components [4].

2.1.4 Navier-Stokes Equations

By letting the control volume in equation (2.5) shrink to an infinitesimal volume one can derive the momentum equation in differential form, also known as Navier-Stokes equations. They are valid for newtonian fluids, which definition is that the viscous stresses are proportional to the element strain rates and the coefficient of dynamic viscosity, μ. For an incompressible flow the Navier-Stokes equations now can be written as

$$\begin{aligned}
\rho\frac{\mathrm{d}u}{\mathrm{d}t} &= \rho g_x - \frac{\partial p}{\partial x} + \mu\Big(\frac{\partial^2 u}{\partial x^2} + \frac{\partial^2 u}{\partial y^2} + \frac{\partial^2 u}{\partial z^2}\Big)\\
\rho\frac{\mathrm{d}v}{\mathrm{d}t} &= \rho g_y - \frac{\partial p}{\partial y} + \mu\Big(\frac{\partial^2 v}{\partial x^2} + \frac{\partial^2 v}{\partial y^2} + \frac{\partial^2 v}{\partial z^2}\Big)\\
\rho\frac{\mathrm{d}w}{\mathrm{d}t} &= \rho g_z - \frac{\partial p}{\partial z} + \mu\Big(\frac{\partial^2 w}{\partial x^2} + \frac{\partial^2 w}{\partial y^2} + \frac{\partial^2 w}{\partial z^2}\Big).
\end{aligned} \tag{2.6}$$

Here ρ denominates the density of the fluid and g is the gravitational constant. u, v and w correspond to velocities in x-, y- and z-direction respectively. By combining these equations with proper boundary conditions and the differential conservation of mass equation (the continuity equation),

$$\frac{\partial u}{\partial x} + \frac{\partial v}{\partial y} + \frac{\partial w}{\partial z} = 0, \tag{2.7}$$

a solution for the velocities u,v, w and the pressure p can be found [4].

2.1.5 Laminar and Turbulent Flow

There are two different kinds of flow: laminar and turbulent. Laminar flow is characterized by a flow that moves smoothly in parallel layers. There is no mixing or flow perpendicular to the layers. Laminar flow moves smoothly around an obstacle in regular paths and occurs at a low Reynolds number.

The flow in nature and in technical applications is turbulent in most cases. The flow becomes turbulent at high Reynolds numbers, when laminar flow becomes unstable. The turbulence is not a property of the fluid, but a property of the flow. Contrary to laminar flow turbulent flow has an irregular movement. Turbulent flow is instationary and has fluctuations that are independent of time and space. This

irregularity means that a lot of computational power would be needed in order to describe the movement of the fluid as a function of time t and the space coordinates x, y, z. The irregularity can be described in such a way that static methods can be used for computing the flow, using time averaged quantities. These static methods have an extra term compared to the equations for laminar flow, which means that assumptions must be made in order to solve these equations.

There are a lot of eddies of different sizes in a turbulent flow field. The eddies are instationary and occur with high intensity. The sizes of the eddies can be as big as the dimensions of the flow field and the size of the smallest eddies are determined by the viscosity of the fluid. The movement of turbulent flow is three dimensional with large fluctuations in the rotational movement. The fluctuations of the velocity are spreading through the surrounding fluid, which means that the turbulence is dissipative. This leads to a high heat transfer and an increased exchange of impulses. Turbulent flow is dissipative, which means that friction in the flow is converted to inner energy of the fluid. Energy has to be provided to compensate these viscous losses in order to maintain the turbulence. If no energy is provided the turbulence would fade out [5].

2.1.6 Reynolds-averaged Navier–Stokes Equations (RANS-equations)

When the studied flow is turbulent the governing equations (for example Navier-Stokes equations) need a lot of computational power to be solved due to small fluctuations of the flow variables (velocity and pressure) in each point in the space of the flow. In absence of the computational power required, assumptions are made to simplify the calculations. The idea is that it is not interesting how these small fluctuations behave but rather how the time-averaged flow variables behave. Therefore these flow variables are divided into two parts, one time-averaged $\bar{(\cdot)}$ and one fluctuating part $(\cdot)'$, as

$$u = \bar{u} + u', \quad v = \bar{v} + v', \quad w = \bar{w} + w', \quad p = \bar{p} + p'. \tag{2.8}$$

If the Navier-Stokes equations (2.6) are evaluated using the formulations in equation (2.8) the result becomes the RANS-equations, which can be written as

$$\begin{aligned}
\rho\frac{\mathrm{d}\bar{u}}{\mathrm{d}t} =& -\frac{\partial\bar{p}}{\partial x} + \rho g_x + \frac{\partial}{\partial x}\Big(\frac{\partial\bar{u}}{\partial x} - \rho\overline{u'^2}\Big) + \\
&+ \frac{\partial}{\partial y}\Big(\frac{\partial\bar{u}}{\partial y} - \rho\overline{u'v'}\Big) + \frac{\partial}{\partial z}\Big(\frac{\partial\bar{u}}{\partial z} - \rho\overline{u'w'}\Big) \\
\rho\frac{\mathrm{d}\bar{v}}{\mathrm{d}t} =& -\frac{\partial\bar{p}}{\partial y} + \rho g_y + \frac{\partial}{\partial x}\Big(\frac{\partial\bar{v}}{\partial x} - \rho\overline{v'u'}\Big) + \\
&+ \frac{\partial}{\partial y}\Big(\frac{\partial\bar{v}}{\partial y} - \rho\overline{v'^2}\Big) + \frac{\partial}{\partial z}\Big(\frac{\partial\bar{v}}{\partial z} - \rho\overline{v'w'}\Big) \\
\rho\frac{\mathrm{d}\bar{w}}{\mathrm{d}t} =& -\frac{\partial\bar{p}}{\partial z} + \rho g_z + \frac{\partial}{\partial x}\Big(\frac{\partial\bar{w}}{\partial x} - \rho\overline{w'u'}\Big) + \\
&+ \frac{\partial}{\partial y}\Big(\frac{\partial\bar{w}}{\partial y} - \rho\overline{w'v'}\Big) + \frac{\partial}{\partial z}\Big(\frac{\partial\bar{w}}{\partial z} - \rho\overline{w'^2}\Big).
\end{aligned} \tag{2.9}$$

The same formulations in equation (2.8) can also be used to evaluate the conservation of mass equation (2.7). The result,

$$\frac{\partial \bar{u}}{\partial x} + \frac{\partial \bar{v}}{\partial y} + \frac{\partial \bar{w}}{\partial z} = 0, \tag{2.10}$$

together with the RANS-equations and appropriate boundary conditions form the basis for solving for the unknown time-averaged flow-variables $\bar{u}, \bar{v}, \bar{w}, \bar{p}$. As can be seen in the RANS-equations (2.9) a couple of new unknowns, $\rho\overline{u_i' u_j'}$ $(i, j = 1, 2, 3 \quad u_1 = u, u_2 = v, u_3 = w)$, have been obtained. These are called turbulent stresses and have to be modelled if the problem is going to be solved, see section 2.1.7.

2.1.7 Turbulence Modelling with Realizable k-epsilon

To solve the RANS-equations in (2.9) the unknown variables, $\rho\overline{u_i' u_j'}$ $(i, j = 1, 2, 3 \quad u_1 = u, u_2 = v, u_3 = w)$, have to be modelled. There are numerous ways of how to perform this modelling and one common used method is the *realizable k-ϵ-model*. This model relates the unknowns, $\rho\overline{u_i' u_j'}$, to the turbulent kinetic energy, k, and the dissipation rate of the turbulent kinetic energy, ϵ, using the Boussinesq assumption:

$$\overline{u_i' u_j'} = -\nu_t \left(\frac{\partial \bar{u}_i}{\partial x_j} + \frac{\partial \bar{u}_j}{\partial x_i} \right) + \frac{2}{3} k \delta_{ij}, \tag{2.11}$$

where $x_1 = x, x_2 = y, x_3 = z$. δ_{ij} is Kronecker delta and ν_t is the turbulent viscosity and is modeled as

$$\nu_t = C_\mu \frac{k^2}{\epsilon}. \tag{2.12}$$

In the *standard k-ϵ-model*, C_μ is a constant determined from experimental results but to get a more accurate estimation of the unknown turbulent stresses a new model, realizable k-ϵ-model, was introduced where this coefficient depends on various properties of the flow. To obtain the turbulent kinetic energy, k, and the dissipation rate of the turbulent kinetic energy, ϵ, two extra transportation equations need to be solved. For exact definitions and a fuller description of the realizable k-ϵ-model the reader is referred to [6].

2.1.8 Separation of Flow

The ideal flow has a boundary layer that follows a blunt body perfectly and attached, as seen in figure 2.1a. However, this is not the case in reality. When the fluid reaches the rear of the body it will experience an increasing pressure gradient that will cause the flow to separate. A turbulent wake develops behind the body with a lower pressure than in the front of the body, see figure 2.1b, which will give rise to a force in the direction of the flow.

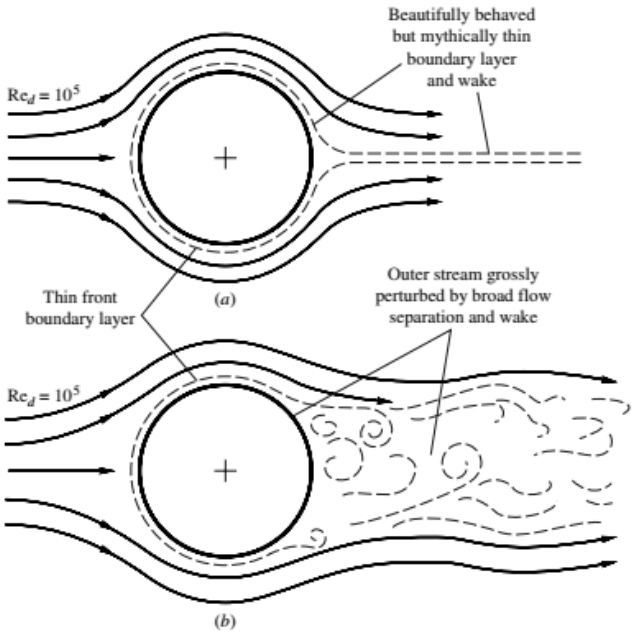

Figure 2.1: *(a) Fully attached flow around a blunt body. (b) Flow that separates at the rear of a blunt body* [4].

When the flow moves across a body that is curved the pressure gradients will change depending on the shape of the body and location of the fluid, which can lead to separation, see figure 2.2. In (1) $\mathrm{d}p/\mathrm{d}x < 0$, which is called a favorable pressure gradient. This means that the flow can never separate from the body. In (2) $\mathrm{d}p/\mathrm{d}x = 0$ and the flow cannot be separated here either. In (3) $\mathrm{d}p/\mathrm{d}x > 0$, known as an adverse pressure gradient, which means that the flow can be separated. However, in this case the gradient is so small that the flow will still be attached. In (4) $\partial u/\partial y = 0$ which means that the separation point is located here. The wall shear stress, τ_w, is zero at the separation point. At (5) the gradient is so strong that a backflow occurs. This causes the boundary layer to thicken greatly and the main flow separates from the wall [4].

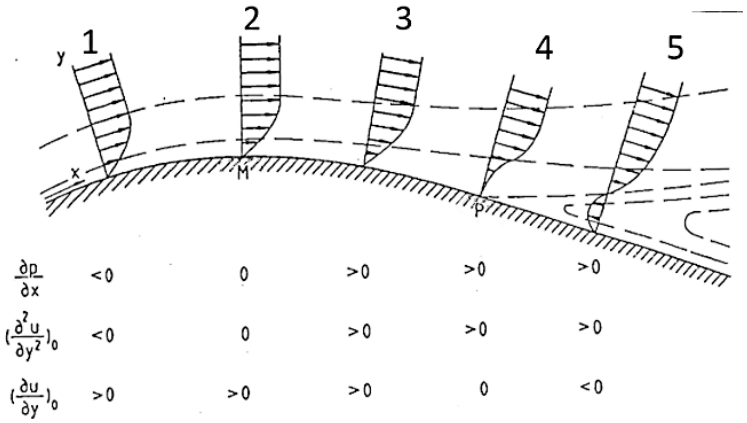

Figure 2.2: *Boundary layers across a curved body, with pressure gradients and velocity gradients defined* [7].

2.1.9 The Boundary Layer Equations

Flow close to the surface of an immersed body is called the boundary layer, where the shear stresses are considerably higher than in the free stream. The boundary layer extends to the point where the outer streamlines velocity is 99% of the free stream velocity. One of the great achievements of this theory is its ability to predict the flow separation that occurs in adverse (positive) pressure gradients. The boundary layer equations are derived from the Navier-Stokes and continuity equations by comparing the magnitude of the included terms in these equations and then applying various simplifications. This results in the following boundary layer equations in two dimensions:

$$\begin{aligned} &\text{Continuity:} && \frac{\partial u}{\partial x} + \frac{\partial v}{\partial y} = 0 \\ &\text{Momentum along wall:} && u\frac{\partial u}{\partial x} + v\frac{\partial u}{\partial y} \approx U\frac{\mathrm{d}\,U}{\mathrm{d}\,x} + \frac{1}{\rho}\frac{\partial \tau_w}{\partial y}, \\ &\text{where the shear stress} && \tau_w = \begin{cases} \mu\frac{\partial u}{\partial y}, & \text{laminar flow} \\ \mu\frac{\partial u}{\partial y} - \rho\overline{u'v'} & \text{turbulent flow} \end{cases} \end{aligned} \tag{2.13}$$

and U is the free stream velocity. If the velocity profile is known the shear stress, τ_w, can also be computed by

$$\tau_w = \rho u^{*2}, \tag{2.14}$$

where u^* is the so called friction velocity. The velocity profile for a turbulent boundary layer varies depending on which region of the boundary layer is in question. The region closest to the surface is called *the viscous sublayer* and is approximated as laminar. The velocity distribution in this region can be approximated by

$$\frac{\overline{u}}{u^*} = \frac{u^* y}{\nu} = y^+, \tag{2.15}$$

where y^+ is a dimensionless coordinate along the boundary layer. Furthermore y is the coordinate normal from the wall, $\bar{u}$ is the time averaged free stream velocity and ν is the kinematic viscosity of the fluid. The viscous sublayer extends from $0 < y^+ < 5$. For $y^+ > 30$ the flow is fully turbulent. This region is called *the log-law region* where the velocity distribution is logarithmic and given by

$$\frac{\bar{u}}{u^*} = \frac{1}{\kappa} ln \frac{u^* y}{\nu} + A \quad \text{where} \quad \kappa \approx 2.44, \quad 4.9 \leq A \leq 5.5. \tag{2.16}$$

The region where $5 < y^+ < 30$ is called *the buffer layer* and neither of the above laws hold in this region.

The boundary layer over a flat plate starts as laminar, hence the local Reynolds number is low in the beginning. At a certain point, called the *transition point*, the boundary layer becomes turbulent, see figure 2.3 below [5].

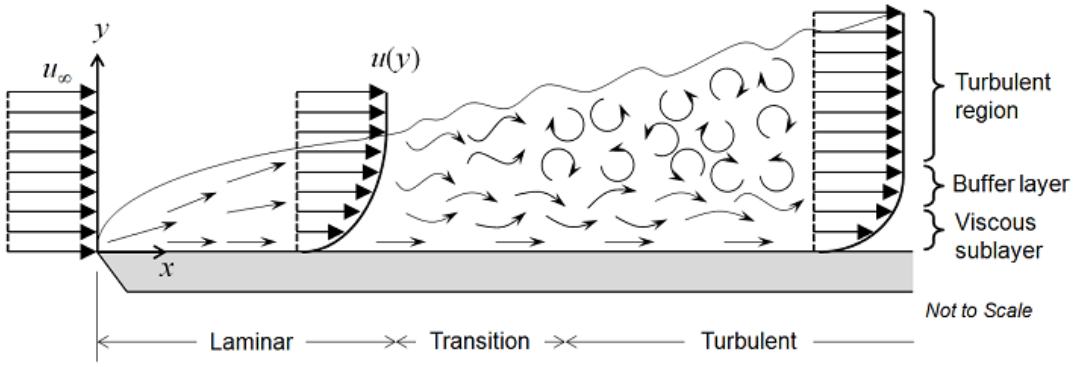

Figure 2.3: *Different regions in a boundary layer for flow over a flat plate* [8].

2.1.10 Drag and Lift Coefficients

A way to compare aerodynamic properties between different bodies is to look at the drag and lift forces. Drag force, F_D, is targeted in the opposite direction as the body's movement and can be seen as a measure of air resistance. It occurs because of the shear stress on the body and the pressure difference between front and rear. Lift force, F_L, measures the force in opposite direction of the gravity, which could cause the body to lift from the ground. Similar to the drag force this is due to pressure differences between the upper and lower sides of the body.

When calculating the drag and lift of various bodies the non-dimensional drag coefficient C_D and lift coefficient C_L are often used, defined as

$$C_D = \frac{F_D}{\frac{1}{2}\rho V^2 A}, \quad C_L = \frac{F_L}{\frac{1}{2}\rho V^2 A}, \tag{2.17}$$

where ρ is the density of the fluid. Furthermore, V is the velocity of the body relative to the fluid and A is the characteristic area, typically the frontal area [4].

2.1.11 Pressure Coefficient

Another parameter that is used to compare aerodynamics between different bodies is the pressure coefficient, C_p. This is the difference between local static pressure, p, and the pressure in the free stream, p_∞, non-dimensionalized in the following way:

$$C_p = \frac{p - p_\infty}{\frac{1}{2}\rho V} \tag{2.18}$$

where ρ is the density of the fluid and V is the velocity of the body relative to the fluid. Contrary to C_D and C_L, C_p is not a coefficient that can show a specific value for the whole body but rather give a local value at different points of the flow [4].

2.1.12 Total Pressure Coefficient

The total pressure, p_{tot}, is the sum of static pressure and dynamic pressure, given by:

$$p_{tot} = p + \frac{1}{2}\rho V^2, \tag{2.19}$$

where ρ is the density of the fluid, p is the static pressure and V is the velocity of the body relative to the fluid. Total pressure coefficient, $C_{p,tot}$, is in turn a dimensionless coefficient that is derived from the total pressure and is given by [9]:

$$C_{p,tot} = \frac{p_{tot}}{\frac{1}{2}\rho V}. \tag{2.20}$$

2.2 Vehicle Aerodynamics

When considering a moving vehicle, both the flow around and through the vehicle as well as the flow concerning the machinery, such as within the engine, has to be taken into account. Regarding the external flow of the vehicle, this field includes both the forces and moments affecting the vehicle but also issues such as how to prevent dirt and water to assemble on the windows and how to reduce the noise that arises from the air passing by. This section will focus on the foundations of vehicle aerodynamics treating the external flow, concentrating on drag force which is one of the main forces affecting the car (drag force is introduced in section 2.1.10). Two other important parts when considering the external flow are the lift force and the forces and moments caused by side winds. Lift force is introduced in section 2.1.10 and is further described below. For an outline of the forces and moments caused by side winds the reader is referred to [9].

2.2.1 Drag Force

Aerodynamic drag is one of the main force components restricting the motion of the vehicle. Therefore, reducing drag is relevant when improving both fuel consumption and speed. As can be seen in equation (2.17), the equation for drag force is given as $F_D = \frac{1}{2}C_D\rho V^2 A$. Hence, the changes that can be made on a vehicle to reduce drag is to decrease the frontal area A and/or the drag coefficient C_D. In general, it is hard to reduce the frontal area since this means that the size of the vehicle has to be reduced. Therefore, the main focus when reducing drag is usually to reduce the drag coefficient [9]. The drag force is the sum of pressure drag and friction drag [4] and focus in this section will be on pressure drag.

When the flow meets the front of the vehicle the velocity decreases and the pressure increases, this area is called the stagnation zone. As the flow moves above the vehicle the pressure decreases as the velocity increases which is described in section 2.2.2. When a viscous flow then encounters the air with higher pressure at the rear of the vehicle the flow separates which results in a low pressure wake behind the body. The difference between the high pressure at the front and the low pressure at

the back of the vehicle gives rise to a significant force in the flow direction [4]. The flow can separate in other places of the body as well, for example where there is a sharp angle, which gives rise to a drag force in the same manner as the wake behind the vehicle.

To prevent wakes from arising and therefore reduce the overall drag, the flow should stay attached to the body as long as possible. This can be done by making the shape of the vehicle streamlined. To reduce the wake at the back of the body, which stands for the highest contribution of the pressure drag, the vehicle should have a slender rear part to make the flow stay attached as long as possible before it is cut off forcing the flow to separate in a controlled way [9].

One way to make the flow stay attached as long as possible is to build a so called boat tail. That is a relatively long, streamlined rear body part with the main function to delay the flow separation. As a consequence the wake area is decreased thus the drag coefficent is reduced [9, 10].

Attaching a cavity at the rear of a car is another way to lower the pressure drag. It is done by attaching an extension that is sufficiently large to the rear end of the car, forming an open frame. This pushes the ring vortex in the wake area further back thus resulting in a higher pressure near the rear of the car. This alternative is more practical and easier to implement than a boat tail [10].

2.2.2 Lift Force

As the air moves above the vehicle the speed of the flow increases, which results in a lift force acting in the direction normal to the motion. For an incompressible and inviscid flow it holds that the sum of the static and dynamic pressure is constant along a streamline. This means that as the speed and the dynamic pressure of the flow increases above the car the static pressure decreases. This results in a lower static pressure above the car compared to under, which gives rise to a lift force. This force has very small effects on the vehicle for velocities below 100 km/h [9].

2.2.3 Example of Drag Coefficient Values

To be able to compare drag coefficients for different cars, some values are presented in table 2.1. The cars presented in this table are examples of cars with rather good aerodynamics compared to other road vehicles. The Volkswagen XL1 from 2011 is a great example of where the aerodynamics has been a main focus. In one article this car is refereed to as "the most aerodynamic production car ever" [11], and similar statements are found in other articles as well.

Table 2.1: Values of C_D for some different car models.

Model	$\mathbf{C_D}$
DTU Dynamo (Shell Eco-marathon participant)	0.14 [12]
Volkswagen XL1, 2011	0.19 [13]
Volvo S60, 2013	0.28 [14]
Toyota Prius, 2012	0.26 [15]
Tesla Model S P85, 2012	0.24 [15]
Mercedes- BENZ CLA250, 2012	0.30 [15]

2.3 Other Relevant Vehicle Dynamics

To be able to describe the total resistance of movement that a vehicle is exposed to while moving, some more factors than just the air resistance need to be taken into account, such as energy lost due to rolling resistance. The energy lost due to rolling resistance is the difference between the work done by the wheel axle, W, and the energy lost due to air resistance. The equation

$$W = s(F_D + F_R) \tag{2.21}$$

can be derived from the reasoning above where s is the traveled distance and F_D is the drag force defined in equation 2.17 in section 2.1.10. Furthermore, F_R is the rolling resistance and a common way of modeling this is to consider it as constant and therefore independent of the velocity [16].

Another factor that needs to be taken into account if the interest is to study the relation between distance and fuel consumption is the efficiency of the powertrain, η. This can be related through

$$E = W/\eta = s(F_D + F_R)/\eta, \tag{2.22}$$

where E is the energy content of the fuel.

2.4 The Finite Volume Method

The finite volume method (FVM) is a numerical method applied to solve partial differential equations [17], and is the most common method used within CFD software. The FVM is based on that the volume of interest is divided into a finite number of small control volumes constituting a volume mesh. The partial differential equations of interest is then solved by integration in each such control volume. This results in a solution in the centroid node of each control volume [18]. Hence, how detailed the final solution is depends on the number of cells. Since the FVM is a numerical method based on an iterative process, the solution obtained can be considered reliable if the iterative process converges [18].

3
Methods

To analyse and improve the original body design of the car Smarter, the method used in this project is computational fluid dynamics (CFD). CFD is used to analyse phenomena related to the flow of a fluid using physical models, numerical methods, software and computers. It makes it possible to indicate the flow around an object without any physical representation of the body. CFD is based on solving the governing partial differential equations within fluid mechanics. The most common method used for this purpose is the finite volume method, which is described in section 2.4.

The workflow of this project can be seen in the flow chart in figure 3.1. In this chart CFD simulations are divided into three stages: pre-processing, processing and post-processing. The pre-processing part was mainly done in the software ANSA and in the processing and post-processing stages the software STAR-CCM+ was used. As seen in the flow chart this project has a type of an iterative process where one design is analysed and then a new design is created. An advantage of using this method is that the framework of the stages included in the iterative process just needed to be established in the first iteration.

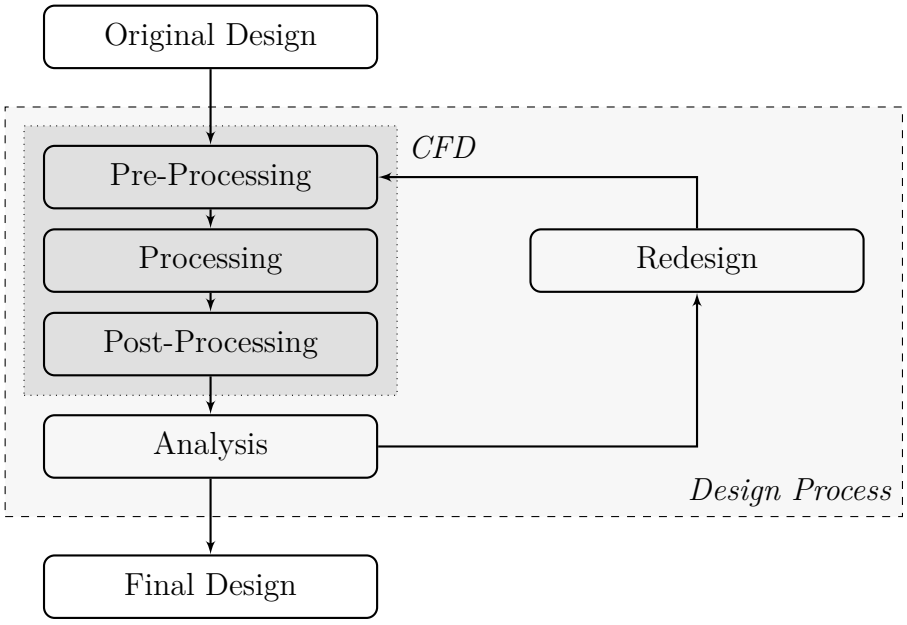

Figure 3.1: *A flow chart of the method.*

3.1 Pre-Processing

A 3D CAD-model had been obtained from the Smarter team and in the pre-processing phase the model was prepared for simulation. The preparations included clean-up operations, categorizing surfaces and finally surface and volume meshing. The pre-processing was needed both for the original CAD-model, received from the Smarter team, and for the CAD-models created later in the project, even though the newer CAD-models needed less pre-processing.

3.1.1 Clean-up Process

When a CAD-model is created, surfaces are defined in a way that is not appropriate for CFD simulations. For example, a closed connection in a CAD software might appear as a gap in a CFD software. This implies that cleaning the geometry is necessary to make the model suitable for a CFD software. In order to clean the geometry, the received CAD-model was imported to the pre-processing software ANSA. The main purpose was to fix errors such as open surfaces and non-manifold edges and vertices. A non-manifold error means that there are multiple connections between edges or vertices. To fix the open surfaces all gaps between surfaces were closed, creating an "airtight" surface. In the process of doing this, one larger simplification had to be made by closing one opening in the undercarriage of the original body design, which is shown in figure 3.2. To eliminate non-manifold errors the number of connections between different edges or vertices were reduced to one. Ignoring these errors would otherwise make the mesh generation inaccurate.

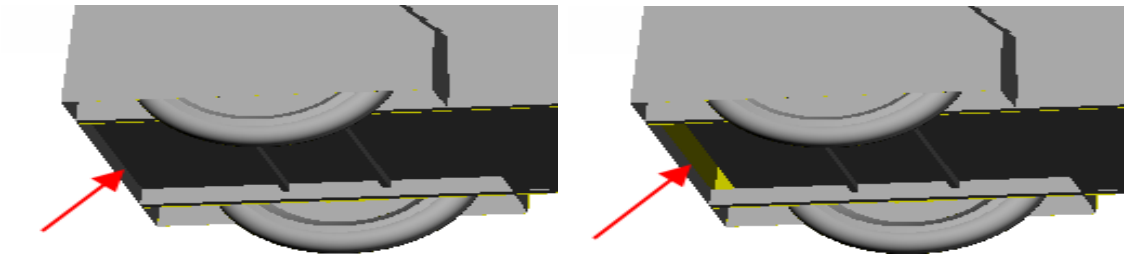

(a) *After closing the opening.* **(b)** *Before closing the opening.*

Figure 3.2: *Comparison of the geometry before and after closing the gap in the undercarriage near the rear wheels of Smarter.*

Since this project aims to analyse only the exterior part of the car all interior parts were removed, creating an empty shell. If the interior parts had been maintained the computational power needed would have been larger than necessary. Also, small parts included in the wheels and wheel suspension and a few areas on the body, containing steps of approximately 1 millimeter, were removed due to meshing limitations, see section 3.1.3.

3.1.2 Categorizing Surfaces

Different phenomena of the flow are expected at different parts of the car. Therefore the surfaces of the car were categorized in different areas, called Property ID:s (PIDs), which can be seen in figure 3.3. These areas were later used to specify how the surface and volume mesh around the car would be created, by defining different cell sizes for the different PIDs. These PIDs were later also used for assigning boundary conditions, e.g. a rotating wheel. However, later in the project it was determined that a different approach of creating refinements in the mesh would be more appropriate to use for this specific case. Therefore only a few of these different PIDs were used to set cell sizes in the mesh.

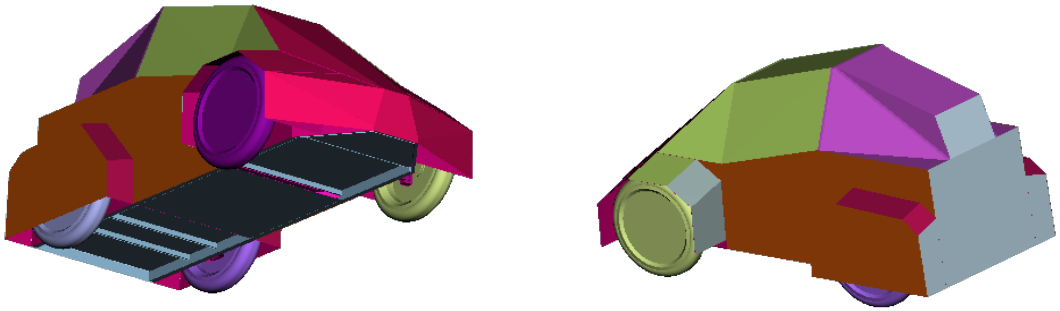

Figure 3.3: *Different PIDs that the car's surfaces were divided into. Note that PIDs with resembling colors might not be the same.*

3.1.3 Meshing

A surface mesh was generated in ANSA as a geometry representation. Some small elements were removed in the clean-up process due to meshing limitations. Some shapes need a very fine mesh to get a correct representation and this requires a high computational power. Since these shapes were considered to have a small impact on the drag they were replaced by similar shapes that are easier to mesh.

With a good representation of the geometry, the model could be imported to the CFD software STAR-CCM+. Two new meshes were then created, a new surface mesh of the car and a volume mesh of the surrounding volume. The surrounding volume was represented as shown in figure 3.4. The large size of the volume was chosen in order to prevent the car from blocking the flow.

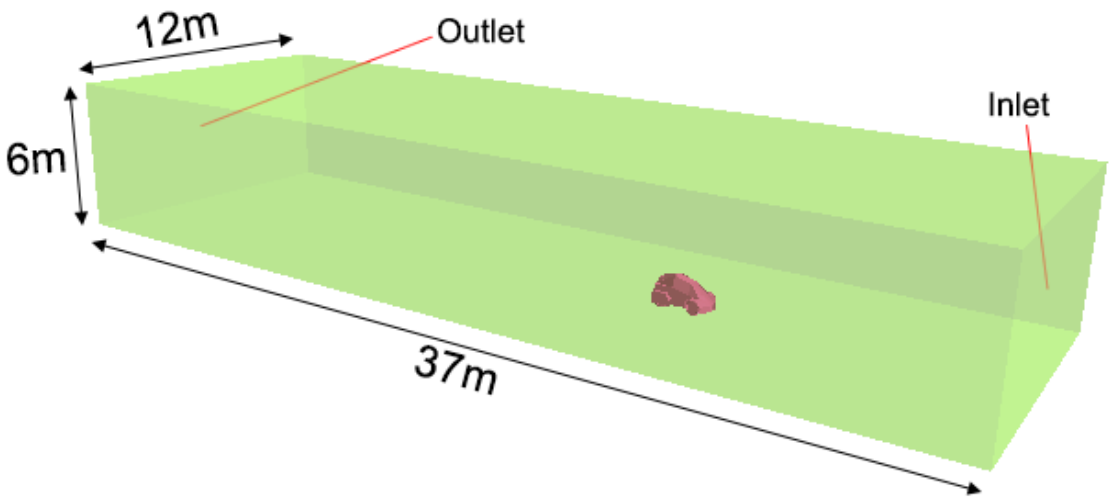

Figure 3.4: *Surrounding volume of the car.*

For the volume mesh a trimmed cell mesher was used which creates cuboid shaped cells. The base size for these cells was set to 8 millimeters. To catch phenomena such as wakes or separation around areas of special interest three refinement zones were placed around the car, see figure 3.5. These zones were assigned to different cell sizes by relating each size to the base.

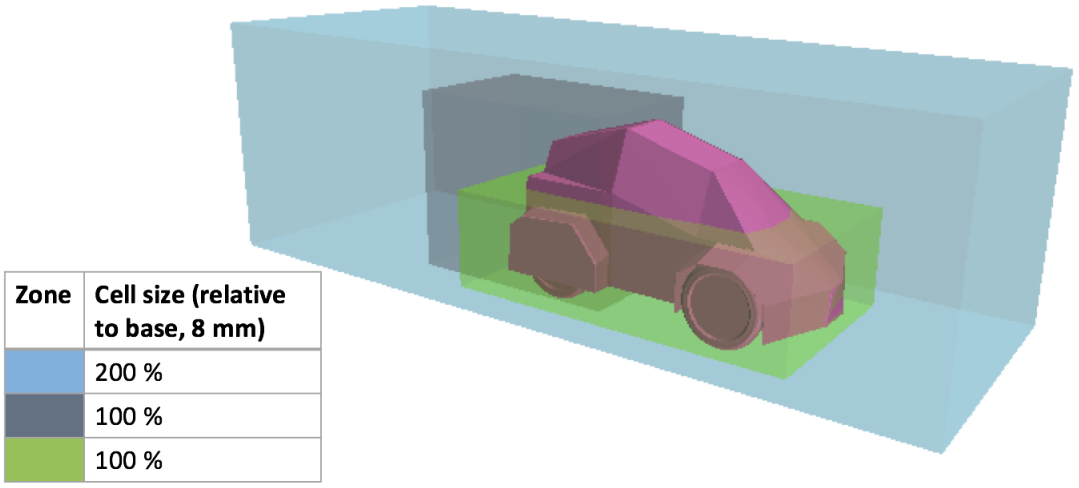

Figure 3.5: *Three refinement zones placed where interesting phenomena can occur.*

3.2 Processing

When the pre-processing phase was completed the simulation was almost ready to run. A few more settings were to be done, including boundary conditions and physical model.

3.2.1 Boundary Conditions

In order to run the simulation boundary conditions were needed to be set. The boundary conditions used can be found in table 3.1. The inlet, outlet, sides, top and floor are referring to the surfaces of the volume surrounding the car seen in figure 3.4.

Table 3.1: Boundary conditions used in STAR-CCM+.

Boundary	**Boundary condition**
Inlet	Velocity inlet at 40 km/h
Outlet	Pressure outlet
Sides	Symmetry
Top	Symmetry
Floor	Wall with velocity set to 40 km/h
Car	Wall
Wheels	Wall with angular velocity corresponding to 40 km/h

3.2.2 Physical Model

The CFD software uses different types of physical models in order to solve different kinds of problems. To get the right solution for this specific case physical models found in table 3.2 were used.

Table 3.2: Physical models used in STAR-CCM+.

Constant Density
Coupled Flow
Exact Wall Distance
Gas (Air)
Gradients
K-Epsilon Turbulence
Realizable K-Epsilon Two-Layer
Reynolds-Averaged Navier-Stokes
Steady
Three Dimensional
Turbulent
Two-Layer All y+ Wall Treatment

3.3 Post-Processing

Post-processing, which means making plots and reports of the result, was done to evaluate the results from the simulations. It was important that every simulation had the same type of post-processing to make it possible to compare the result from each simulation. A number of different data types, like plots, graphs and reports,

were defined. The chosen types made it possible to compare the different designs and see where improvements in the aerodynamics could be made.

Plots and data types used in the post-processing:

- Velocity distribution of the flow
- Pressure coefficient, C_p, as a contour plot on the car
- C_D vs length of the car, both accumulated and local values
- Total pressure coefficient, $C_{p,tot}$, as an isosurface on the car
- Values of C_D and C_L

3.4 Analysis and Redesign

The results from the post-processing needed to be analysed in order to find problem areas that could be improved. New designs were made in the CAD software Autodesk Inventor Professional.

3.5 Mesh Dependency Study and Computational Resources Determination

When using CFD, a critical part of the process is to know how fine the mesh should be. If the mesh is too coarse the result will be inaccurate due to inability to capture the full behaviour of the flow. If the mesh is too fine the time for calculations will be long due to computing power restrictions. Therefore a goal in every CFD project is to find a mesh as coarse as possible that still captures all the behaviours of interest. A common way to establish this is to refine the mesh until the studied variables do not change more than can be tolerated. This tolerance can be different in different types of studies and is often based on experience.

In this project a baseline mesh was created. The baseline mesh had a base size of 8 mm which resulted in a mesh consisting of approximately 15 million cells. To be able to establish if this was an appropriate base size two new meshes were created, one coarser and one finer. For the coarser mesh a base size of 10 mm was used, which resulted in approximately 8 million cells, and for the finer mesh a base size of 6 mm was used, which resulted in approximately 30 million cells.

With the three different meshes mentioned, the flow was calculated. In each of the three cases the calculations had reached convergence after roughly 3000 iterations. To compare the data resources needed for the different meshes CPU-time was used, which is a way to quantify the time for simulations. The resulting computational time was around 240 CPU-hours for the baseline mesh, 140 CPU-hours for the coarser mesh and 510 CPU-hours for the finer mesh.

The variables C_D and C_L of each calculation were then extracted and compared, see table 3.3. To obtain a clear overview of the difference of these values a plot

presenting the correlation of the studied variables and the cell count was made, see figure 3.6. As can be seen in both the table and the figure the variable of main interest, C_D, is stable and does not vary more than around three thousandths. The other variable of interest C_L is not as stable as C_D but through discussion with the supervisor of this project it was decided that this variation could be tolerated.

Table 3.3: Relation between the refinement of the mesh and variables of interest.

Base size	Cell count	CPU-time	C_D	C_L
6 mm	29 626 370	510 h	0.424	-0.057
8 mm	14 828 920	240 h	0.427	-0.050
10 mm	8 570 234	140 h	0.427	-0.057

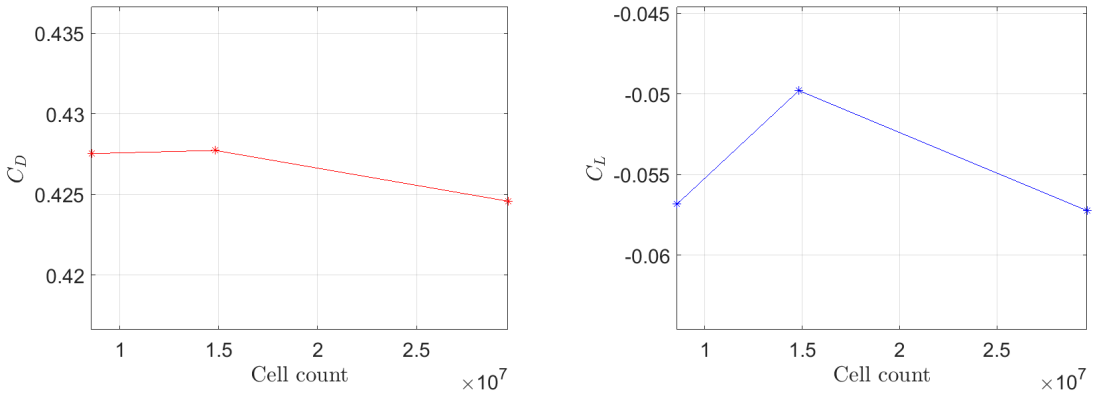

(a) *Correlation of cell count and drag coefficient.*

(b) *Correlation of cell count and lift coefficient.*

Figure 3.6: *Correlation of force coefficients and cell count.*

The next step of the mesh dependency study was to determine which of these three base sizes that was to be used for all of the remaining CFD calculations of this project. The base size of the baseline mesh (8 mm) was selected since it had been shown that it was not too coarse for capturing the flow behaviour of interest. Other flows that were to be simulated during the project may need a finer mesh in order to capture all interesting phenomena and get the right values for the studied variables. This is the reason for not choosing the grossest mesh, since some margins are preferable.

4
Original Design

In order to distinguish the areas that needed improvement, simulations had to be done on the original body design of Smarter. The original body design can be seen in figure 4.1. The frontal area of the original design is $0.9784\,m^2$ and the rest of the primary dimensions can be found in section 1.4.3.

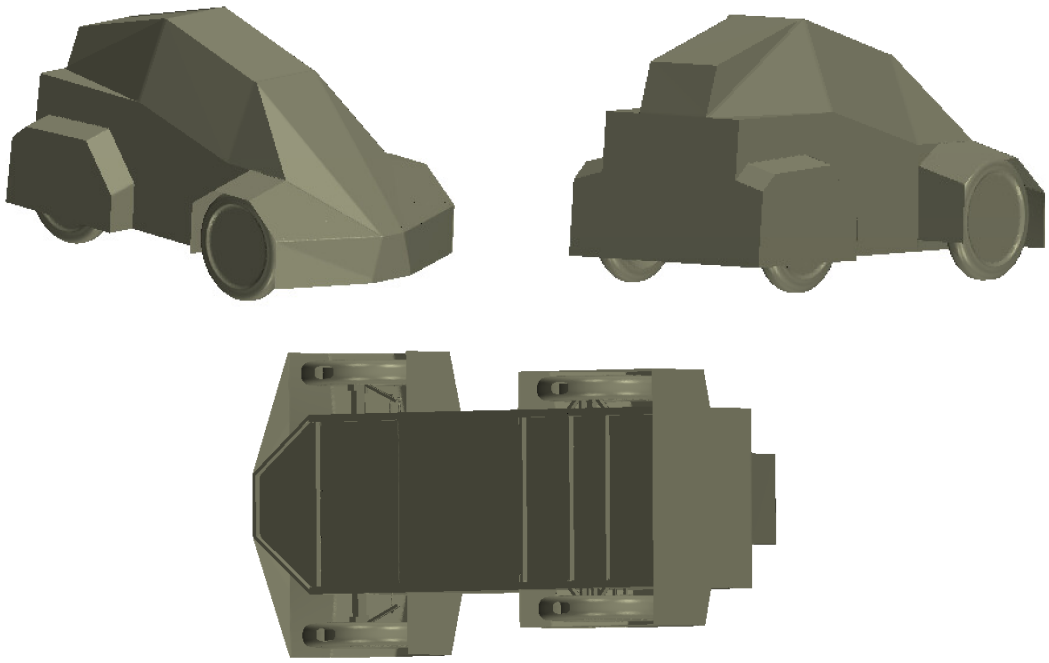

Figure 4.1: *Original body design of Smarter.*

After running simulations on the original body design the aerodynamic properties were analysed. Problematic areas could be spotted through velocity distribution plots, pressure coefficient contour plots, isosurfaces of $C_{p,tot} = 0$ and values of C_D and C_L. The drag coefficient, C_D, was calculated to a value of 0.427 and the lift coefficient, C_L, was calculated to -0.050. Figure 4.2 shows a histogram over C_D along the x-axis of the car. Each red bin corresponds to a local C_D which contributes to the total value. The histogram shows that the largest contributions to drag appears to be at the front and the rear of the car.

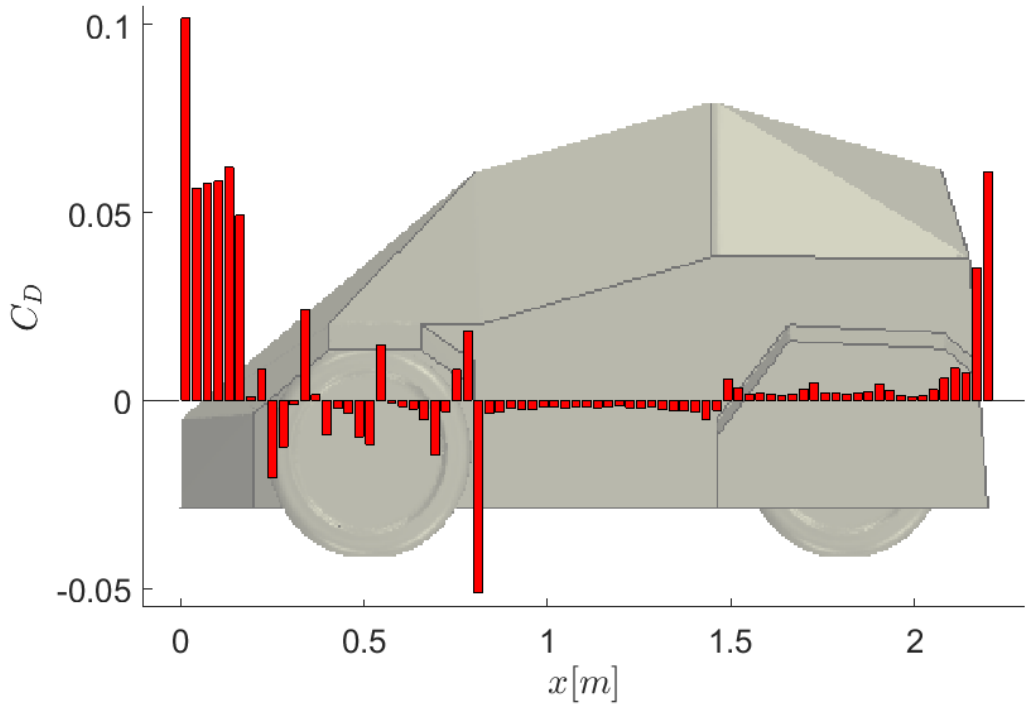

Figure 4.2: *Histogram showing the local drag coefficient, C_D, along the x-axis of the car. The accumulated C_D is 0.427.*

A contributing factor to the aerodynamic drag is the separation of flow which gives rise to losses in the flow. In figure 4.3 an isosurface illustrates where the total pressure coefficient is equal to zero, which corresponds well to where wakes are formed. Wakes can be seen as the green "bubbles" surrounding the car and are formed mainly around the front wheel fenders, around the A-pillars and behind the car.

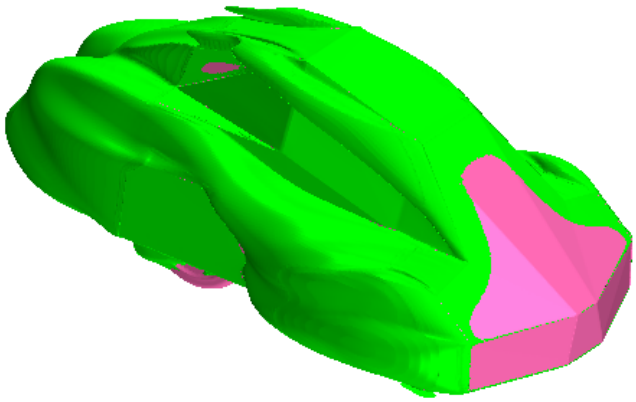

Figure 4.3: *Smarter with an isosurface of $C_{p,tot} = 0$ showing where wakes appear.*

The wakes can also be studied with a velocity distribution scene. In figure 4.4 the velocities of the flow are shown. Blue color indicates low speed and areas with this color coincide with areas where wakes are formed. In figure 4.4a velocity distribution in a plane that is located 35 cm above the ground clearly shows recirculation in wakes around the front wheel fenders (marked by arrows) as well as a wake behind the car. Figure 4.4b shows a similar scene but in a side view of the car. Here the wake behind the car is visible. In figure 4.4c the car is shown from behind. The plane which shows the velocity distribution is a cross section of the car approximately 15 cm from the rear end. The two shapes that appear as "ears" on the top of the car are vortices with origin around the A-pillars.

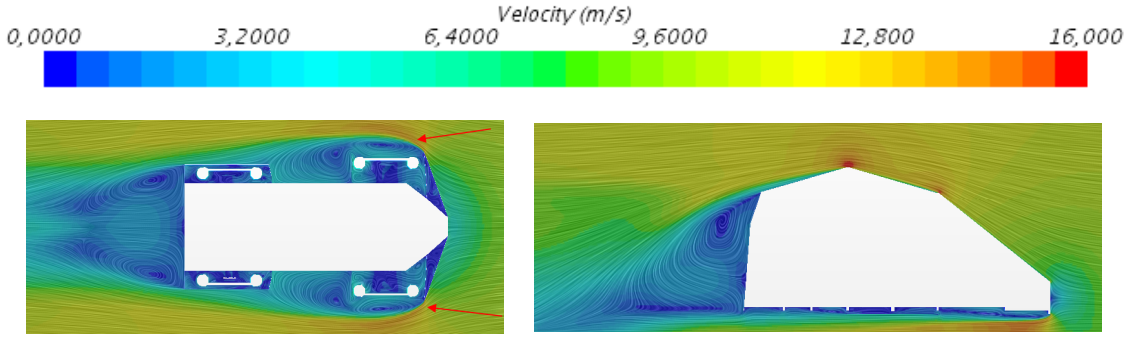

(a) *Smarter seen from above. The velocity is shown in a plane that is located 0.35 m above the ground. Wakes around the fenders of the front wheels are marked by arrows. Also the wake behind the car is visible.*

(b) *Smarter seen from the right side. The wake behind the car can be seen.*

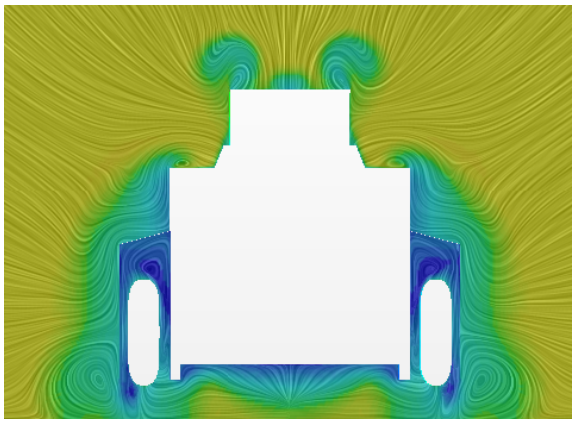

(c) *Smarter seen from behind. The velocity is shown in a plane that is located 0.15 m from the rear of Smarter. The two "ears" just above the car are the vortices formed by the A-pillars.*

Figure 4.4: *Velocity distribution scenes.*

When studying the velocity distribution scenes more closely two more areas with large energy losses in the flow were discovered. The car has an undercarriage with exposed beams which disturb the flow. On the top of the car a small plateau causes the flow to separate. Both of these phenomena can be seen in figure 4.5.

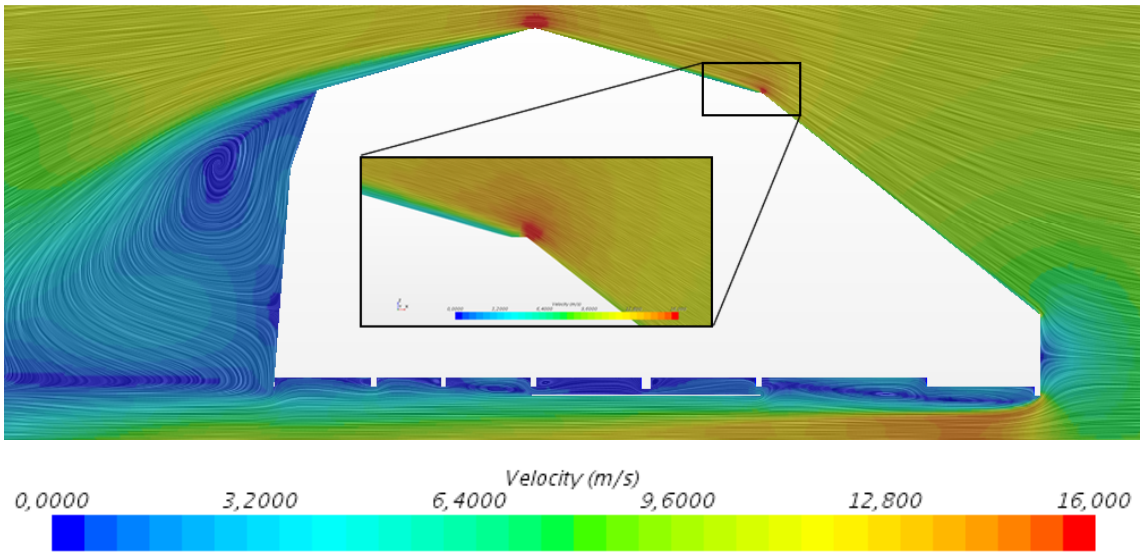

Figure 4.5: *Smarter seen from the right in a velocity distribution scene. The beams of the undercarriage, which cause a disturbance in the flow, can be seen as white dots below the car. The part that is zoomed in shows the plateau which causes the flow separation.*

In order to see the pressure distribution on the car the images in figure 4.6 can be used. Figure 4.6a shows the pressure coefficient, C_p, on the front of the car. The maximum pressure is seen as a red area at the front of the car. In figure 4.6b pressure distribution on the car is shown from behind.

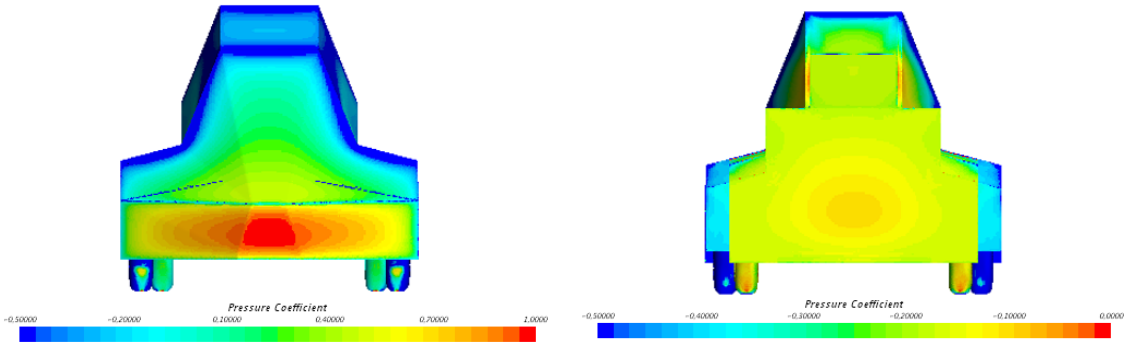

(a) *Smarter shown from the front.* **(b)** *Smarter shown from behind.*

Figure 4.6: *Pressure coefficient, C_p, on the body of Smarter. Note the difference between the two scales.*

5
Design Process

This chapter presents designs and analysis of the modifications made during this project. When the original design had been analysed new designs were created with intention to reduce the drag of the car. The design process started with making small changes in the original design which resulted in a new standard to use for all new designs. Focus was then put on changing the front of the car, which resulted in a second standard. This second standard was then used when proceeding to reshape the rear. Ultimately some other small modifications were made and analysed. The design process concluded in a final design, presented in chapter 6. During the design process two major sum ups of the different analysed designs were done. The first one was done after the front modifications and the second one was done after the rear modifications. In these sections the drag coefficient and the frontal area, which does not affect C_D but the total drag force, are presented. The lift coefficient, C_L, will not be presented for each modification since the impact is small for velocities below 100 km/h, as mentioned in section 2.2.2. However, a comparison of C_L between the original and the final design will be made in chapter 6.

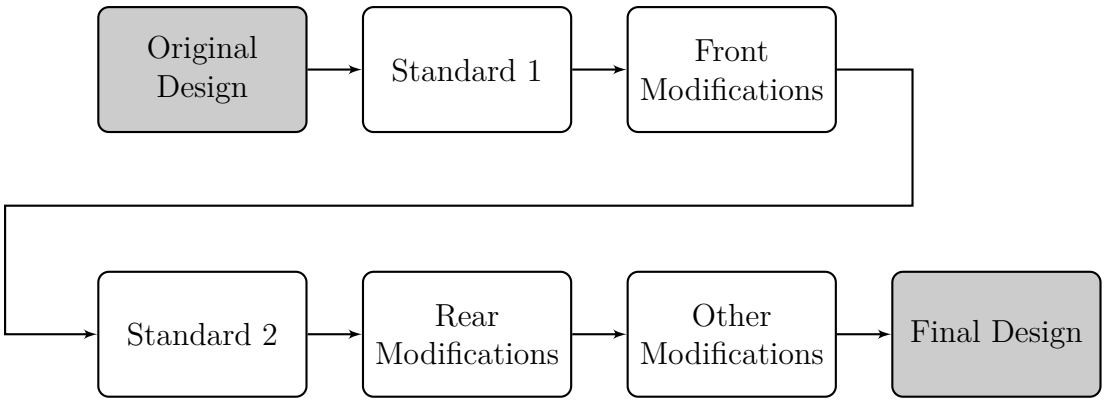

Figure 5.1: *A flow chart of the steps in the design process. Note that the grey boxes are separated sections and not part of the design process.*

5.1 Standard 1

To start the design process some obvious improvements to the original design of Smarter were done. A simple change was made eliminating the problems concerning the undercarriage and the plateau. By adding a flat plate to the undercarriage the beams were covered up and a reshape on the top of the car eliminated the

plateau. The changes can be studied in figure 5.2.

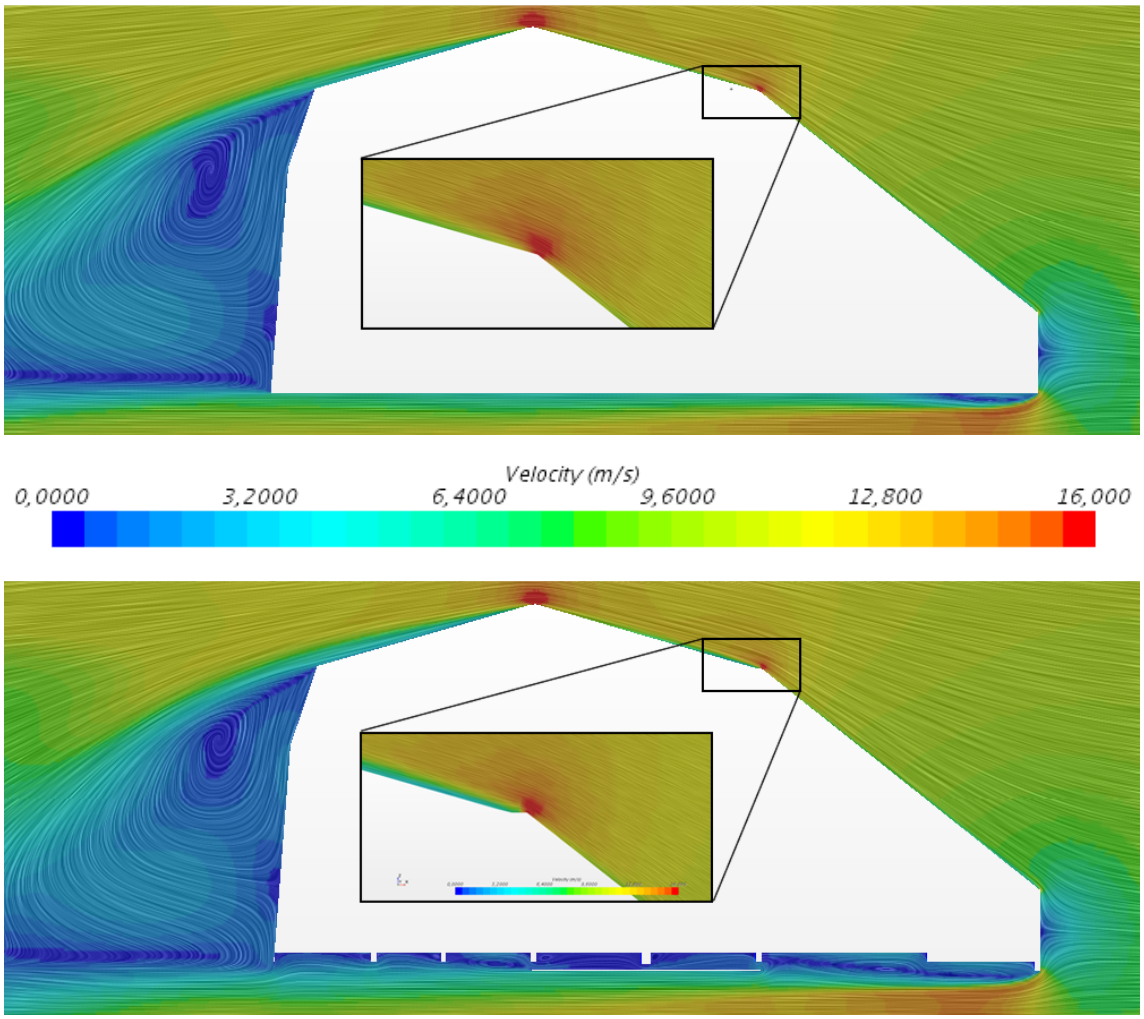

Figure 5.2: *Comparison of the velocity distribution between standard 1 (above) and the original design (below) seen from the right side. The plateau at the roof has been removed and the beams in the undercarriage have been covered up.*

These small changes eliminated the small separation along the roof and made the flow stay better attached along the undercarriage, which in turn led to a slightly smaller wake behind the car. This design lowered C_D to a value of 0.379. Compared to the original design with a C_D of 0.427 this was a decrease by 11%. This new model was considered a new standard, "standard 1", upon which all following changes in design were made.

5.2 Front Modifications

The first larger modifications of Smarter focused on reshaping the front part in order to avoid vortices and separation around the A-pillars and the front wheel fenders. Focus during the front modifications was also to reduce the stagnation zone at the

front. Even though changes could be made in the rear part these changes would be insignificant if the separation occurred upstream.

5.2.1 Short Nose Shaped Front

The original design of Smarter has a flat front which causes a relatively large area to be exposed to high pressure. In order to reduce this area, a design with a nose shaped front was introduced. This smooth shape of the front also makes the air stay attached longer downstream which results in a lower drag coefficient. The geometry can be seen in figure 5.3.

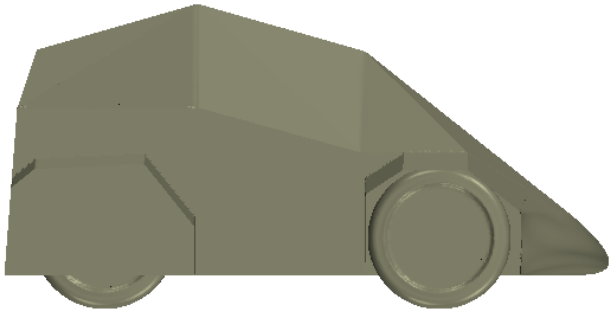

Figure 5.3: *Geometry of the short nose shaped front seen from the side,* C_D = 0.378.

The new C_D was computed to 0.378, which is a small decrease in value compared to standard 1 having a C_D of 0.379. The stagnation zone at the front of the car was reduced compared to the original design as can be seen in figure 5.4.

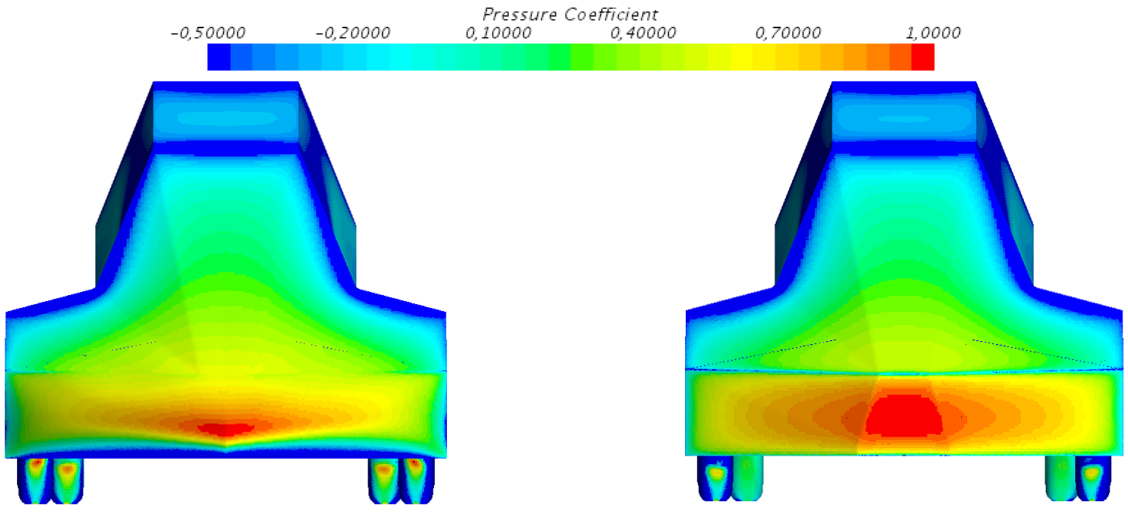

(a) *Short nose shaped front.* **(b)** *Standard 1.*

Figure 5.4: *Comparison of the pressure coefficient,* C_p*, on the front of the two different designs. Note that the stagnation zone has decreased for the short nose shaped front compared to Standard 1.*

5.2.2 Long Nose Shaped Front

Similar to the short nose shaped front this configuration aims to reduce the area exposed to high pressure and make the air stay attached longer along the sides of the car. Contrary to the short nose this change requires more work to implement as the whole front must be redesigned. The geometry can be seen in figure 5.5.

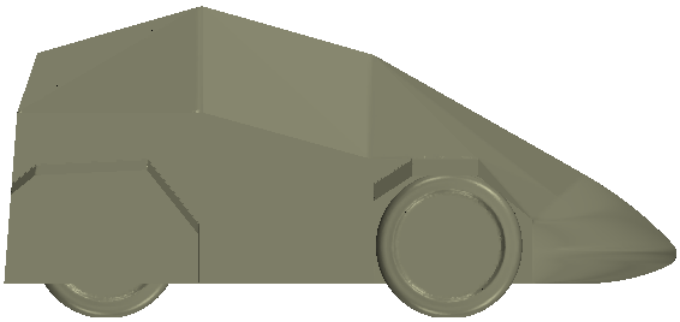

Figure 5.5: *Geometry of the long nose shaped front as seen from the side,* $C_D = 0.337$.

After running the simulation a C_D of 0.337 was obtained. Figure 5.6 shows the isosurface of $C_{p,tot} = 0$ of the new design compared to standard 1. A significant difference in separation around the A-pillars and the front wheel fenders from standard 1 can be seen.

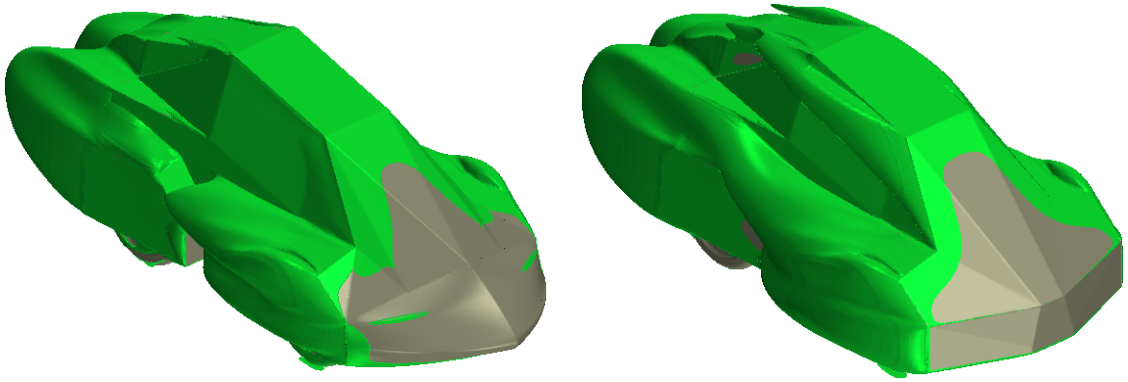

(a) *Long nose shaped front.*

(b) *Standard 1.*

Figure 5.6: *Isosurfaces of* $C_{p,tot} = 0$ *on geometry of the two different designs. Note the difference in wakes behind the A-pillars.*

With this design the stagnation zone in the front was reduced in a similar way as for the short nose shaped front.

5.2.3 Rounded Front Wheel Fenders

The fenders of Smarter have many edges where the flow separates. To make the air stay attached longer, the front fenders were reshaped to a smoother design, see

figure 5.7. These changes were only made on the front fenders since the current configuration only focuses on changing the front of the car.

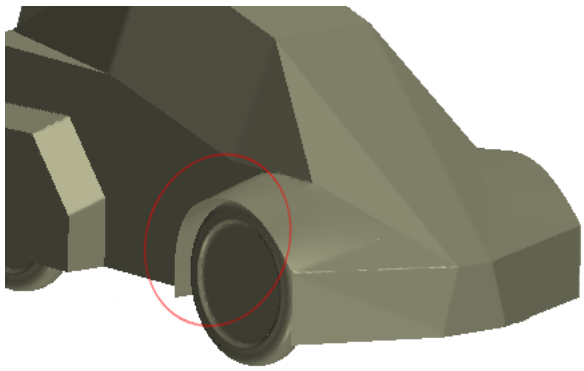

Figure 5.7: *Geometry of the rounded front wheel fenders, $C_D = 0.574$. The change in design is marked.*

The smoothness of the back of the fenders gave rise to larger wakes on the sides of the car, which resulted in an increase of C_D to 0.574. The isosurface of $C_{p,tot} = 0$ of the original design and this design can be seen in figure 5.8.

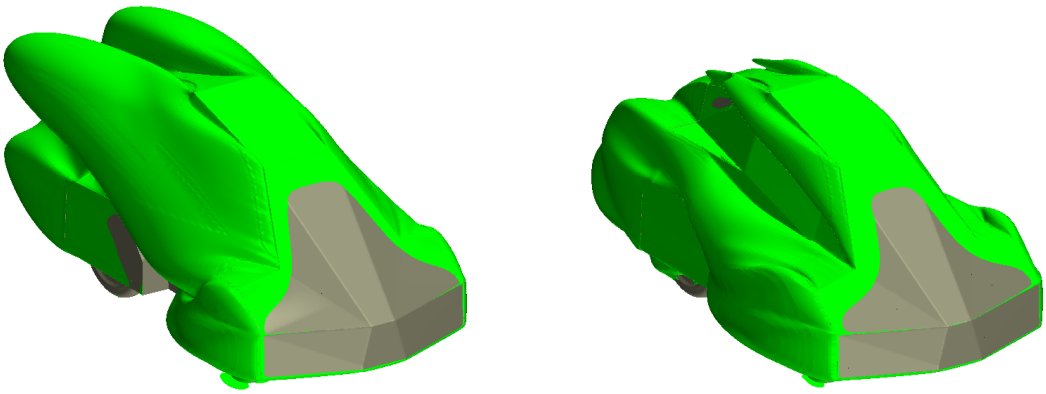

(a) *Smoothed front wheel fenders.* **(b)** *Standard 1.*

Figure 5.8: *Isosurface of $C_{p,tot} = 0$ on geometry of the two different designs. Note that the smoothed front fenders give larger wakes behind the front wheels.*

5.2.4 Rounded A-pillars

The analysis of the original design shows a vortex formation and early separation of flow around the A-pillars. This is caused by the sharp angle of the A-pillars in the original design, in combination with the fact that the sides of the car currently have a slight angle inwards. This inflection makes the angle that the incoming air encounters as it flows around the A-pillars larger than if the sides were flat, which in turn makes it harder for the flow to stay attached. Therefore, in order to reduce the separation at this section, the A-pillars were smoothed and the inwards angle of the sides was removed, making the sides of the car flat, see figure 5.9. When flattening the sides, the roof was extended slightly. Additionally, in order to perform

the rounding operation without changing the overall design of the front, the front wheel fenders were raised slightly. The radius of the A-pillars was set to 90 mm, a value that was chosen to obtain the wanted result without obstructing the driver's sight.

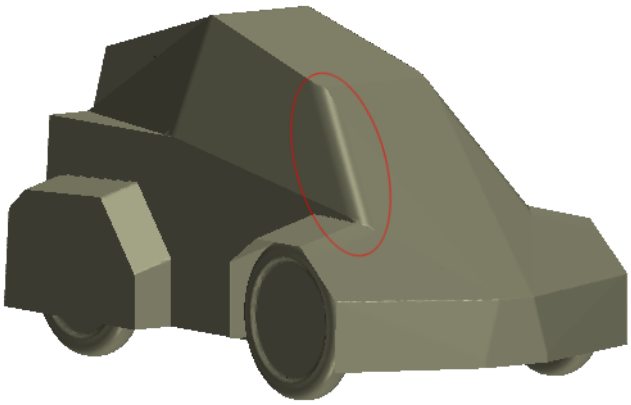

Figure 5.9: *Geometry of the car with rounded A-pillars and flattened sides,* $C_D = 0.379$*. The change in design is marked.*

The isosurface $C_{p,tot} = 0$ of this modification can be seen in figure 5.10. It is obvious that the vortices around the A-pillars were decreased which resulted in lower drag in this area. Nevertheless, the total drag on the car, which was computed to 0.379, did not differ from the drag on standard 1. The reason for this is probably the development of larger wakes downstream, caused by the changes done.

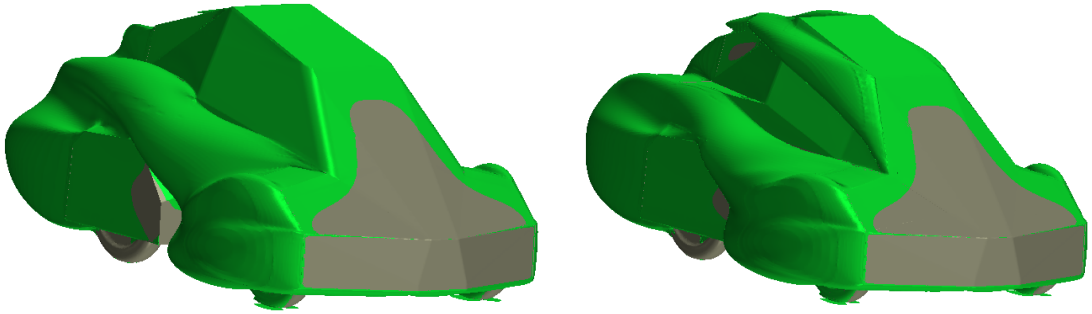

(a) *Rounded A-pillars.* **(b)** *Standard 1.*

Figure 5.10: *Isosurface of* $C_{p,tot} = 0$ *on geometry of the two different designs. Note especially the difference in the region around the A-pillars.*

5.2.5 Sum up of Front Modifications

After the front modifications were done it was quite obvious that the long nose shaped front was preferable due to it giving by far the largest reduction of the drag coefficient. This configuration resulted in lowering C_D by 11% compared to standard 1. The reason for not combining the modification of the A-pillars with the

long nose shaped front was that the vortices eliminated by the rounded A-pillars also disappeared when extending the front.

In order to compare the different configurations the accumulated drag coefficient, C_D, is plotted versus the length of the car, x, in figure 5.11. The total value of C_D and the frontal area for the different designs is listed in table 5.1.

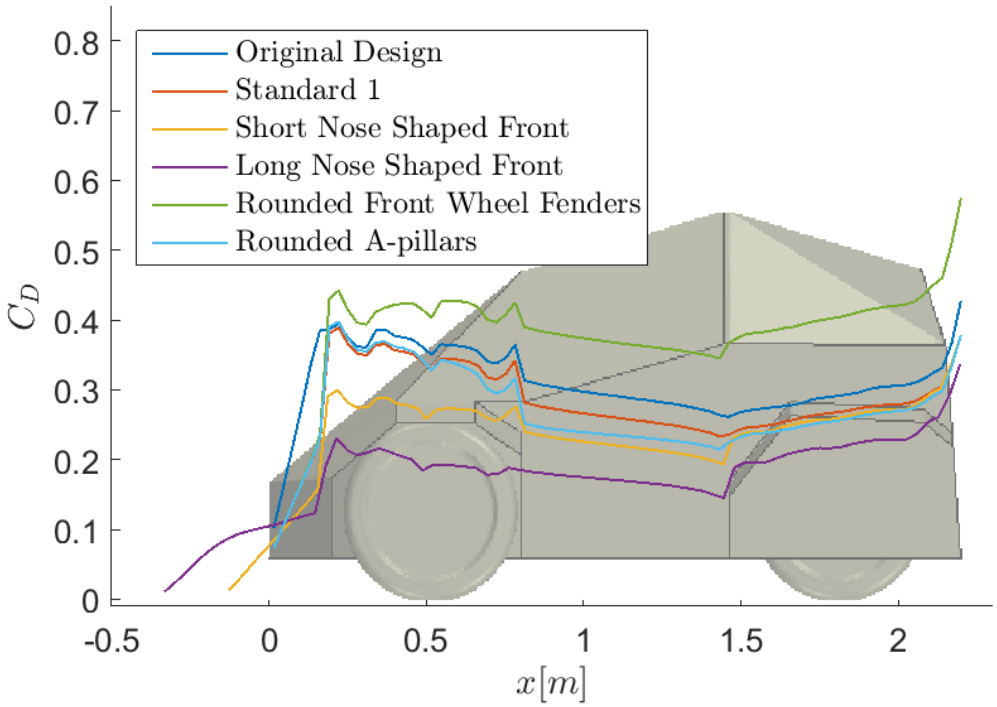

Figure 5.11: *Accumulated drag coefficient, C_D, plotted versus the length of the car, x, for the configurations made during the front modifications. This graph shows how different areas of the car contributes to the total drag coefficient.*

Table 5.1: Values of C_D and frontal area for different configurations made during the front modifications. The lowest value of C_D is marked with a grey background.

Design	**C_D**	**Frontal area [m^2]**
Original Design	0.427	0.9784
Standard 1	0.379	0.9783
Short Nose Shaped Front	0.378	0.9784
Long Nose Shaped Front	0.337	0.9783
Rounded Front Wheel Fenders	0.574	0.9833
Rounded A-pillars	0.379	0.9781

Overall the design with the long nose shaped front gave a satisfying flow around the front of the car with a lower C_D. Despite the relatively big changes in design for

the Smarter team to implement, this was chosen to be the configuration to proceed from when starting to reshape the middle and rear part of Smarter.

5.3 Standard 2

When the front modifications of the body were established a new standard, "standard 2", was created where some obvious improvements were done. This design would later be used to base the rear configurations on.

First of all a new long nose shaped front design with "sharper" end angle of the body in front of the front wheels was created to get a smaller wake around these areas, see figure 5.12a and 5.12b. Another change was to remove the open space between the front wheel fenders and the back wheel fenders. This was done in order to make the flow stay better attached, which was a problem in the earlier configurations. The design of standard 2 can be seen in figure 5.12c.

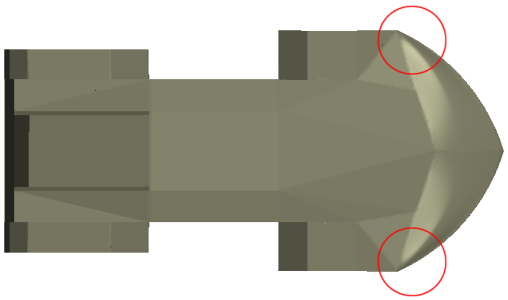

(a) *Long nose shaped front from above. The circles illustrate the end angle.*

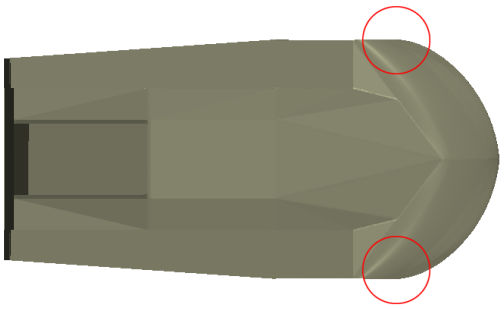

(b) *Standard 2 from above. The circles illustrate where the end angle has been sharpened.*

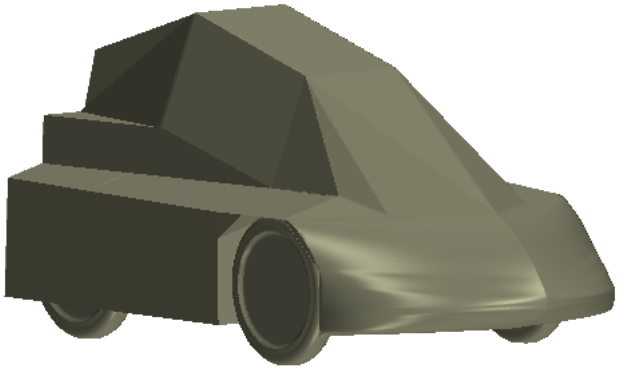

(c) *Design of standard 2.*

Figure 5.12: *Standard 2, (b) and (c), $C_D = 0.237$. Note the sharper end angle of the front for standard 2 compared with the long nose shaped front in (a).*

This change in design reduced the drag coefficient significantly. The result of standard 2 is a drag coefficient of 0.237, compared with the long nose shaped front with a C_D of 0.337, which is a decrease of 30%. The original design had a C_D of 0.427, which means that standard 2 has reduced the drag coefficient with 44%. In figure 5.13 the velocity distribution of the flow shows that the flow stays better attached when connecting the two fenders.

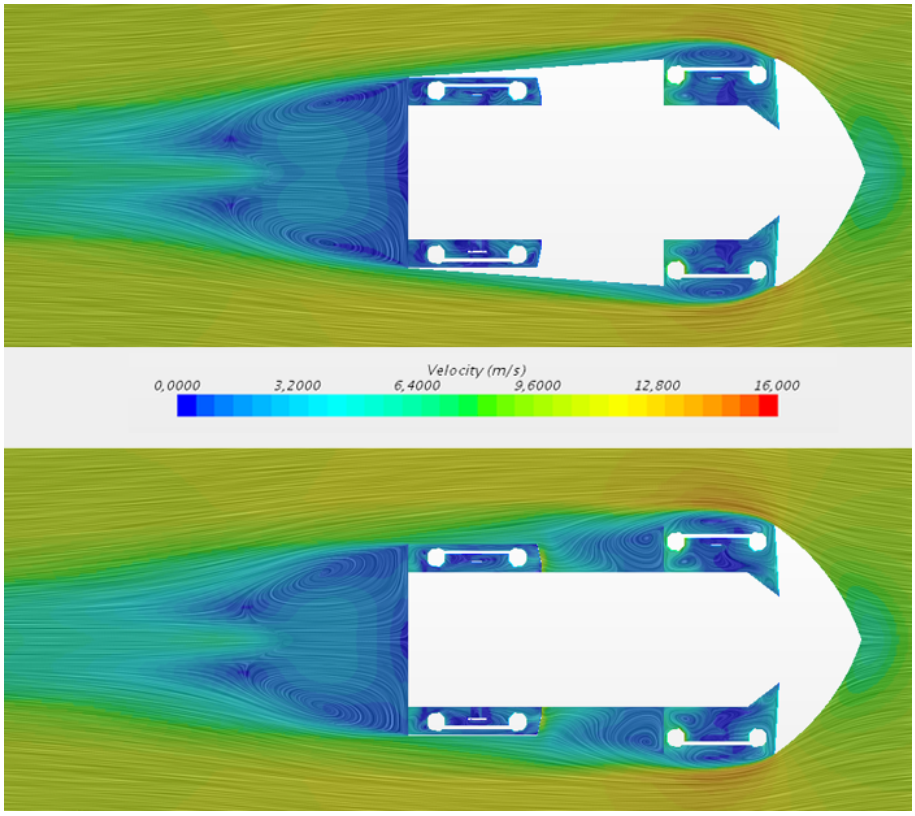

Figure 5.13: *Velocity distribution of the flow around standard 2 (above) and the long nose shaped front (below) seen from above. The velocity is shown in a plane that is located 0.35 m above the ground. Note that the flow is better attached along the side of the vehicle in standard 2.*

5.4 Rear Modifications

After various front modifications the next step was to reshape the rear part of the vehicle, using standard 2 as a basis. Analysis of the flow around standard 2 shows that separation still occurs in the middle and the rear part of the body, something that creates pressure drag. The most significant contribution to the pressure drag is the wake behind the car. The aim when reshaping the rear part was hence to avoid the separation that occurs at the middle and rear part of the body and to reduce the wake behind the car.

5.4.1 Edgy Boat Tail

The large wake area behind the car was the main focus of this configuration. One of many ways to reduce the wake area is to taper the rear end of the car by attaching a boat tail. The concept of this design was to make a boat tail which consists of flat plates to simplify manufacturing. This design was achieved by extending the floor and attaching new plates to the rear and connecting them at a point further back, see figure 5.14. The length of the tail was limited to 100 cm to satisfy the regulations of the competition. Furthermore, to prevent the flow from separating at the beginning of the tail, the angle at the transition between the body and the boat tail could not be too big. The tapering was abruptly cut at the end to insure a controlled separation.

Figure 5.14: *Geometry of the edgy boat tail,* $C_D = 0.168$.

The drag coefficient, C_D, on this configuration was 0.168 which is a lower value compared to standard 2 having a C_D of 0.237. Figure 5.15 shows the velocity distribution of the flow around the vehicle which indicates that the flow seems to stay attached to the boat tail except for minor separations in the beginning. Note that the wake area behind the car has been significantly reduced.

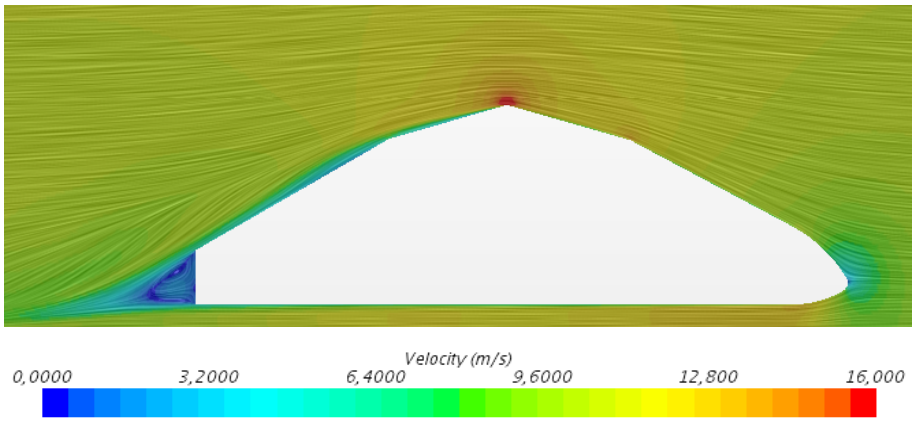

Figure 5.15: *Velocity distribution around the edgy boat tail seen from the right side.*

5.4.2 Rounded Boat Tail

After the encouraging result from the edgy boat tail the next step was to improve it. This was done by giving it a more rounded form. Numerous different designs of this type were created to evaluate the best shape. The alterations made to the designs consisted mainly of changing the area and height at the end of the boat tail. The design which gave the most satisfying flow can be seen in figure 5.16. In addition to the boat tail two minor changes were done in this configuration. The roof was rounded to further prevent separation, which can be seen in figure 5.16c. Also the "catwalks" were removed which can be seen in figure 5.16b. The "catwalks" are the protruding plateaus on the sides of the rear, these are marked in figure 5.16a.

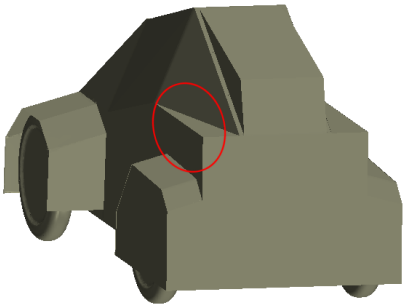

(a) *The "catwalks" from the original design.*

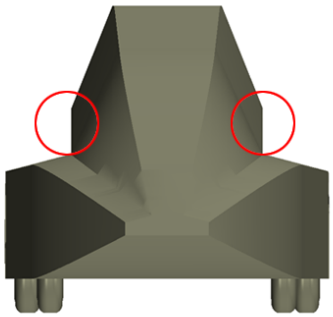

(b) *Geometry of the rounded boat tail seen from the back. The red circles indicate where the "catwalks" have been removed.*

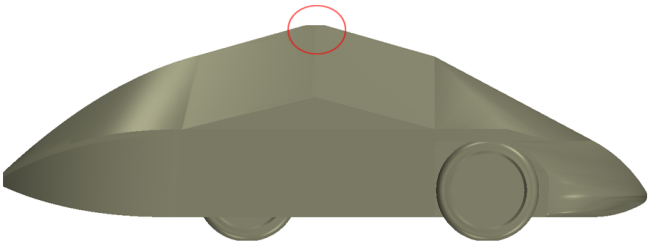

(c) *Geometry of the rounded boat tail seen from the side. The red circle indicates where the roof has been rounded.*

Figure 5.16: *Geometry of the rounded boat tail, $C_D = 0.152$, and a figure of the original design showing where the "catwalks" have been removed.*

These changes lowered C_D to a value of 0.152. Also, the wake behind the car was reduced compared to the edgy boat tail design, as can be seen in figure 5.17, showing the velocity distribution.

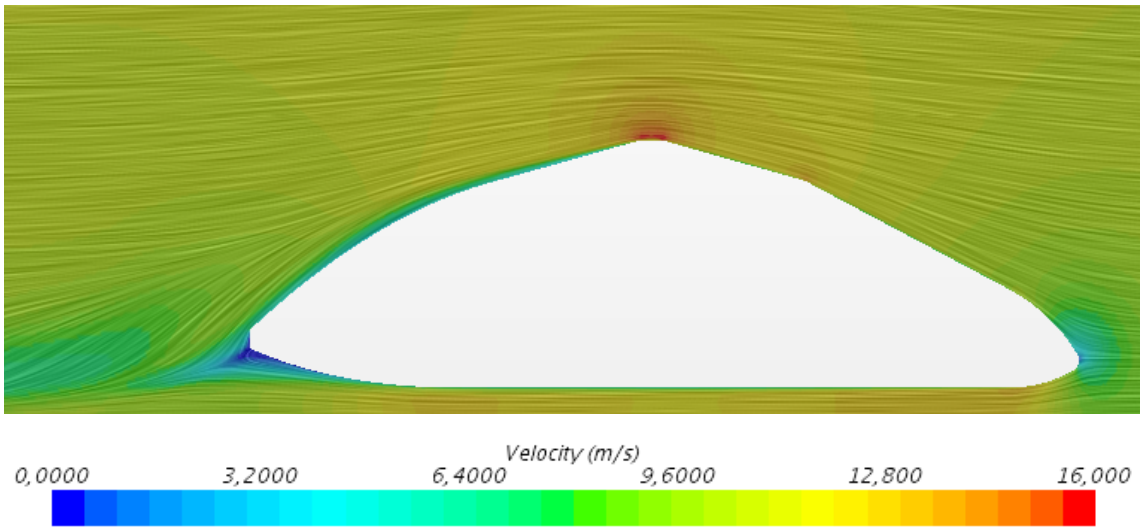

Figure 5.17: *Velocity distribution of the rounded boat tail design seen from the right side. Note the small size of the wake behind the vehicle.*

The wake behind this design is almost non-existent, as seen in figure 5.15, which was the aim of adding the boat tail. An advantage with this design is the decreased separation zone along the back of the roof, once again compared with the edgy boat tail design.

5.4.3 Rounded Top and Reduced Rear Wheels Opening

To prevent the air from flowing into the rear wheel arches, the undercarriage around the rear wheels was extended, see figure 5.18a. This configuration also had a rounded roof as in the rounded boat tail, see figure 5.18b. The last modification of this design was to remove the "catwalks", also in the same way as the rounded boat tail, as can be seen in figure 5.16a and 5.16b. This configuration was done in order to see what result these minor changes gave, without any major change included.

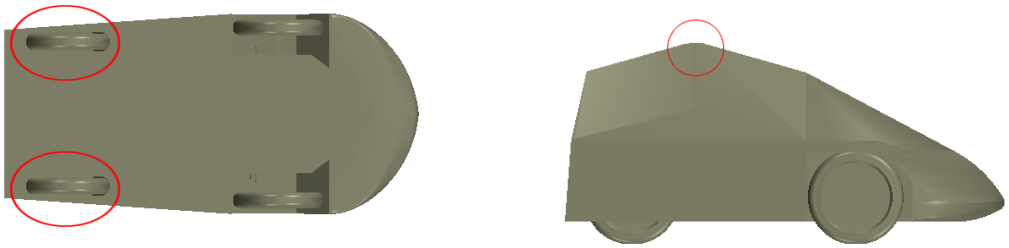

(a) *Reduced wheels opening in the undercarriage around the rear wheels.*

(b) *Rounded top.*

Figure 5.18: *Rounded top and reduced opening around the rear wheels. This design also included removing the "catwalks",* $C_D = 0.221$.

These changes resulted in a C_D of 0.221, which is an improvement compared to standard 2 with a C_D of 0.237. The major changes of the flow were reduced wakes, illustrated with the isosurfaces of $C_{p,tot} = 0$ in figure 5.19 and 5.20.

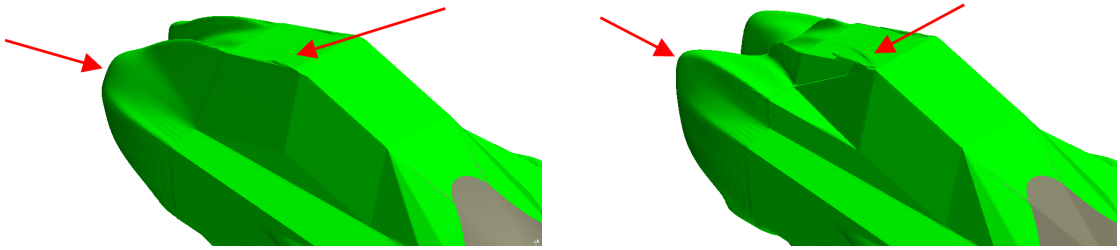

(a) *Rounded top and reduced rear wheels opening.* **(b)** *Standard 2.*

Figure 5.19: *Isosurfaces of $C_{p,tot} = 0$ on the roof of the two different designs. Note the differences in the wakes which occur along the roof and behind the car marked by the arrows.*

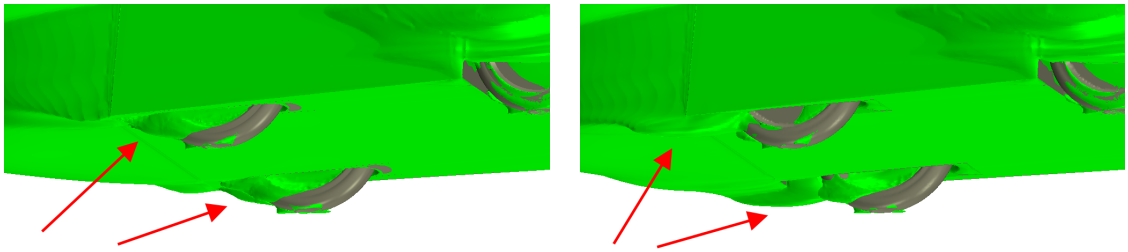

(a) *Rounded top and reduced rear wheels opening.* **(b)** *Standard 2.*

Figure 5.20: *Isosurfaces of $C_{p,tot} = 0$ on the undercarriage of the two different designs showing the rear wheels. Note the difference in the wakes marked by the arrows.*

5.4.4 Cavity

Another approach instead of using a boat tail in order to reduce the drag in the rear part is to use a cavity. The cavity was made by extending the back of the car with an open section, as seen in figure 5.21. This configuration also includes the changes with the rounded top and reduced opening around the rear wheels. The cavity is easy to implement and does not demand much material or extra weight.

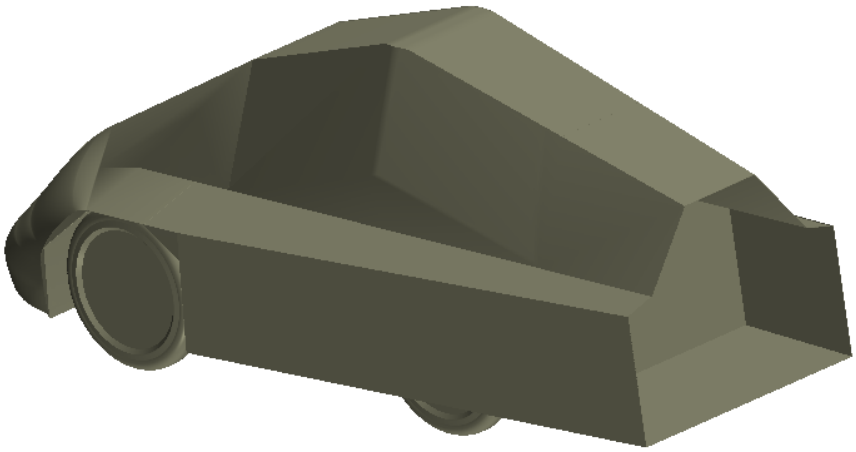

Figure 5.21: *Geometry of the cavity attached at the rear of the car,* $C_D = 0.196$.

This configuration resulted in a C_D of 0.196. Without the cavity C_D was 0.221, which means that the cavity had an improved effect on the drag reduction. The expected positive effect when adding a cavity was increased pressure at the rear of the car. This was achieved and is shown in the pressure coefficient scenes in figure 5.22. The reason for the increased pressure is that the vortices in the wake behind the vehicle occur further away from the back of the vehicle, which is shown in the velocity distribution scene in figure 5.23.

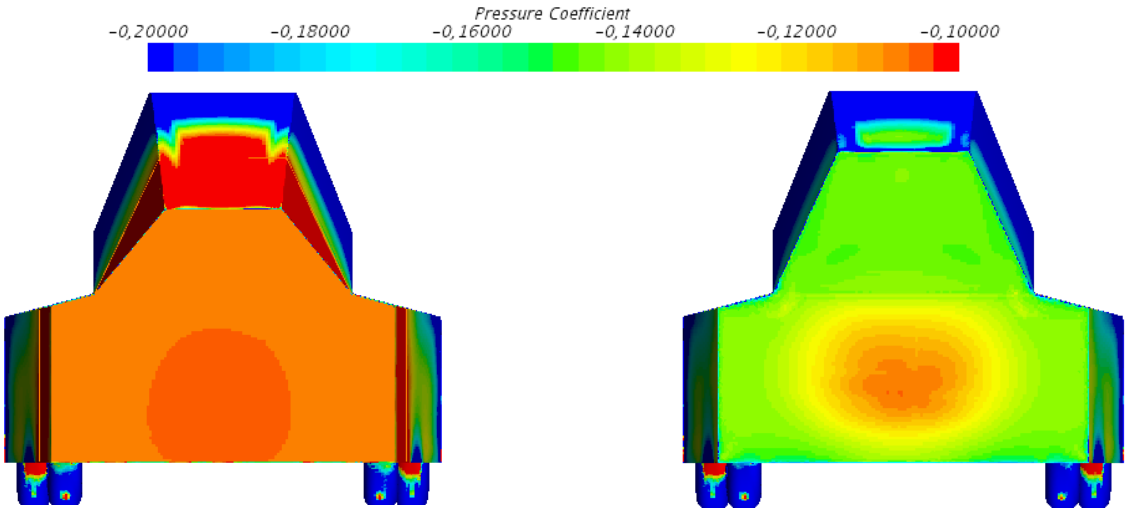

(a) *Cavity.*

(b) *Rounded top and reduced rear wheels opening.*

Figure 5.22: *Pressure coefficient on the rear of the car. Note the increased pressure on the cavity design.*

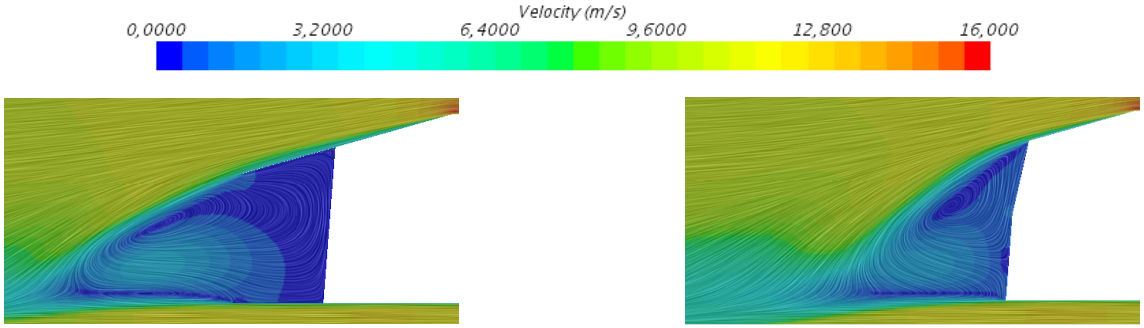

(a) *Cavity.*

(b) *Rounded top and reduced rear wheels opening.*

Figure 5.23: *Velocity distribution at the rear of the car, seen from the right side. Note that the vortices occur further away from the back at the cavity design.*

5.4.5 Sum up of Rear Modifications

When summing up the rear modifications it can be concluded that the rounded boat tail was the configuration resulting in the best improvement regarding drag coefficient, with a decrease of 36% compared to standard 2. The second best improvement was received with the edgy boat tail, with a decrease of 29%, which indicates that the configurations with boat tails constitute the best improvements.

The accumulated drag coefficient, C_D, is plotted versus the length of the car, x, in figure 5.24 and the total value of C_D and the frontal area for the different designs is listed in table 5.2.

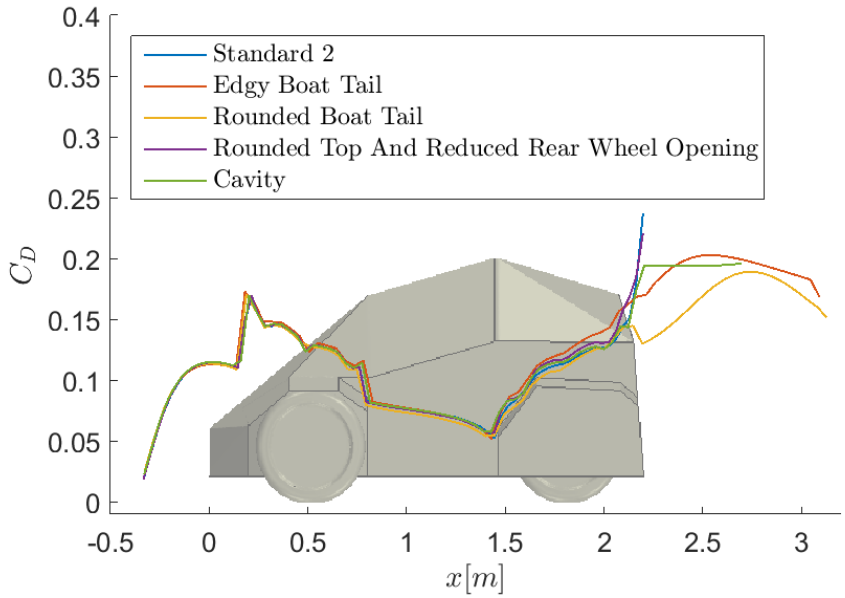

Figure 5.24: *Accumulated drag coefficient, C_D, plotted versus the length of the car, x, for the configurations made during the rear modifications.*

Table 5.2: Values of C_D and frontal area for different configurations made during the rear modifications. The lowest value of C_D is marked with a grey background.

Design	**C_D**	**Frontal area [m^2]**
Original Design	0.427	0.9784
Standard 2	0.237	0.9786
Edgy Boat Tail	0.168	0.9790
Rounded Boat Tail	0.152	0.9733
Rounded Top and Reduced Rear Wheels Opening	0.221	0.9728
Cavity	0.196	0.9728

In addition to the rear modifications presented above some other configurations were done which are presented in section 5.5. When taking these into consideration it could still be concluded that the rounded boat tail gave the best improvement regarding drag coefficient among the configurations that were done after standard 2. Hence, the rounded boat tail constituted the foundation to the final design.

5.5 Other Modifications

In addition to the modifications already presented some smaller alterations of the design were made that will be introduced in this section. These configurations were based on standard 2.

Two different modifications were made to the "catwalks" without having any other part of the body reshaped. The area in question is marked in figure 5.25a. One of the modifications was to cover the empty spaces above the "catwalks" by flat plates, which can be seen in figure 5.25b. This was done in an attempt to avoid the vortices that arise from the "catwalks". However, this alteration also resulted in a larger area at the rear. The resulting C_D of this design was 0.243, compared to standard 2 with a C_D of 0.237.

The other modification made to this area, without changing any other part of the car, was to remove the "catwalks" and replace them with flat plates. The new design can be seen in figure 5.25c. The aim of this was, in addition to avoid the vortices arising from them, also to reduce the area at the rear end and in that way make the wake at the back smaller. Analysis of the results shows that the flow still stayed attached to the body until it was cut off at the rear. The resulting value of C_D of this configuration was 0.229, compared to standard 2 with a C_D of 0.237.

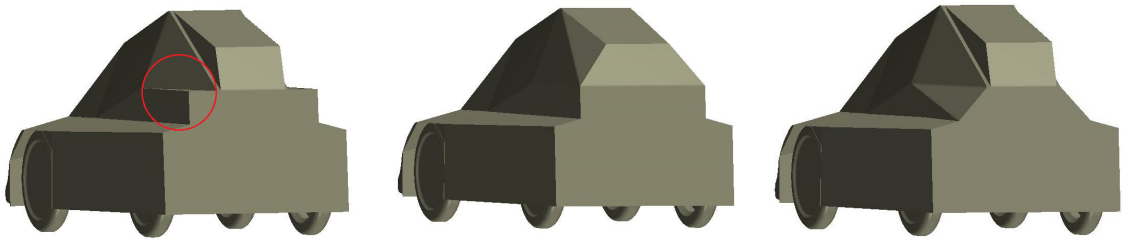

(a) *Geometry of standard 2 with a "catwalk" marked on one side,* $C_D = 0.237$.

(b) *Geometry of the car after adding plates covering the empty spaces over the "catwalks",* $C_D = 0.243$.

(c) *Geometry of the car after removing the "catwalks" and replacing them with flat plates,* $C_D = 0.229$.

Figure 5.25: *The "catwalks" on the sides of standard 2 marked and the design of two modifications that were made on these areas.*

Another modification was to add front wheel deflectors in order to force the air to flow on the sides and under the wheels instead of into the wheel arches. The deflectors were 10.5 cm broad, 2.3 cm high and placed 4 cm from the outer edge of the wheel fenders. These measurements were still within the regulations of the competition considering ground clearance, which can be found in section 1.4.2. The design resulted in a C_D of 0.244. This was an increase of drag coefficient compared to standard 2, with a C_D of 0.237. The isosurfaces of $C_{p,tot} = 0$ around the front wheel of the design with wheel deflectors and standard 2 can be seen in figure 5.26. This figure shows a new wake behind the front wheel deflector.

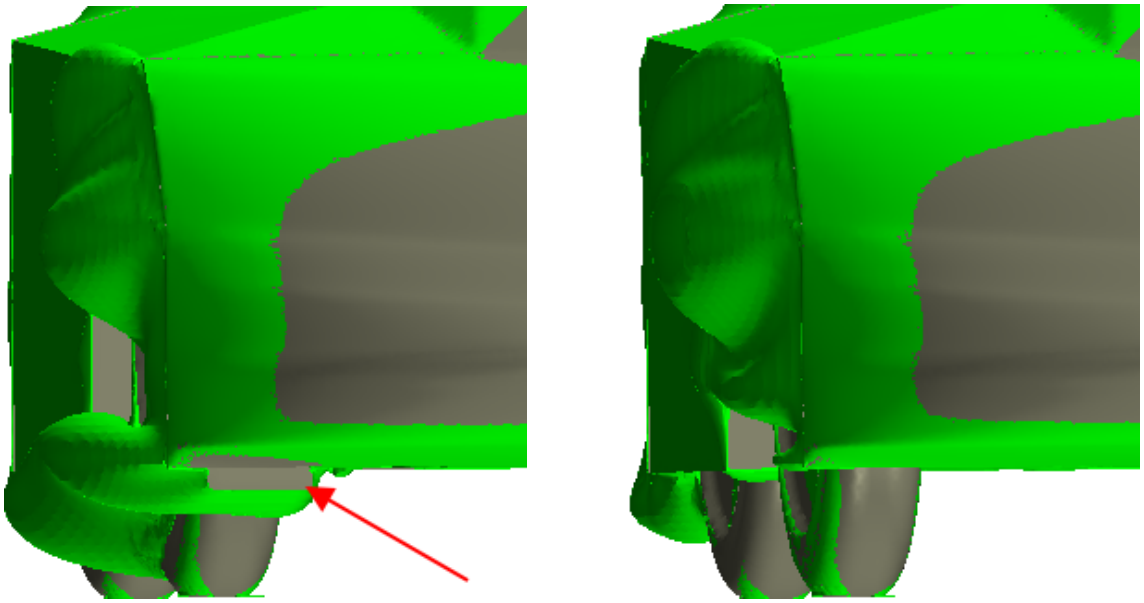

(a) *Front wheel deflectors. The arrow points at the wheel deflector.*

(b) *Standard 2.*

Figure 5.26: *Isosurfaces of* $C_{p,tot} = 0$ *of the areas around the front wheel. Note the new wake behind the front wheel deflector.*

6
Final Design

This chapter presents a final design. This design is based on modifications presented in the design process. A comparison with the original design considering both the geometry and the aerodynamics is included.

6.1 Geometry

The configurations made in the design process were all based on the the original design. This implies that the final design also is based upon the original geometry. Hence, even though there are major differences between the original and the final design there are still similarities. The geometry of the final design is shown in figure 6.1.

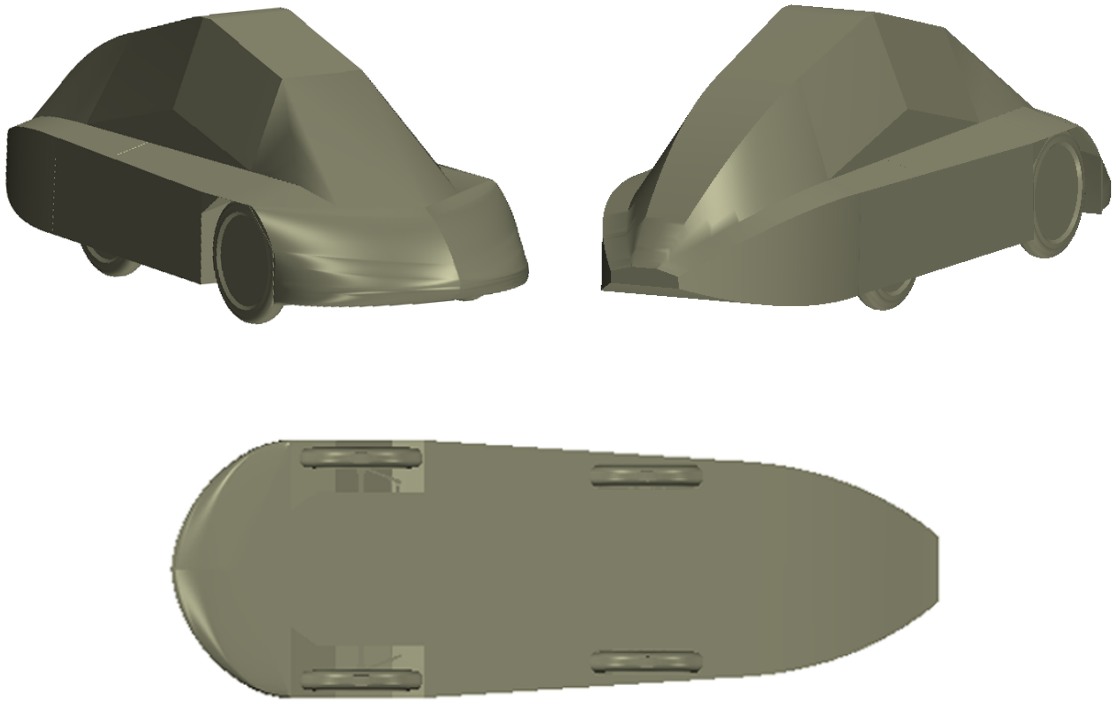

Figure 6.1: *Three views of the final design.*

The final design is a combination of two different designs described in the design process. The main part of the design originates from the rounded boat tail, pre-

sented in section 5.4.2, which in turn is based on standard 2 in section 5.3. This is combined with the configuration with closed floor around the rear wheels, described in section 5.4.3. This led to a heavily reduced drag, with a C_D of 0.146, compared to the original design, with a C_D of 0.427, which is a reduction of 66%. The lift coefficient, C_L, changed from -0.050 for the original design to -0.039 for the final design.

Most of the final design is built on rather simple geometries, seen from a construction point of view. The reason for this is the delimitations regarding the manufacturing process, which is described in chapter 1.3. The possibility to manufacture the final design will be discussed in section 7.

The primary dimensions of the final design are presented in figure 6.2. These dimensions fulfill the corresponding regulations of the competition, listed in section 1.4.2. The frontal area of the vehicle changed from $0.9784\,m^2$ for the original design to $0.9733\,m^2$ in the final design.

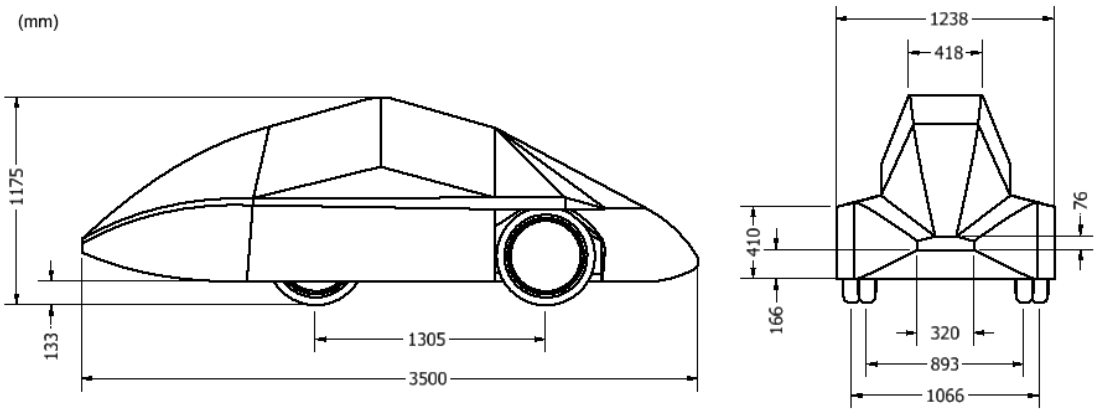

Figure 6.2: *Dimensions of the final design, side and rear view.*

The changes made to the final design compared to the original design are summarized in a numbered list below. Each of the changes mentioned in the list is also marked with a corresponding number in figure 6.3, where both the final and the original design are presented to enable comparison.

The changes made are:

1. The beams in the undercarriage have been covered up by adding a flat plate.
2. The small plateau on the roof right behind the windshield has been eliminated.
3. The front, including the windshield, has been reshaped. The windshield are still made out of flat surfaces, but the front has a more complex geometry.
4. The front fenders have been connected to the rear fenders by flat plates. The size and geometry of the wheel arches have been kept from the original design.
5. The top of the roof has been rounded.
6. The openings between the rear wheels and the surrounding undercarriage have been reduced.

7. A boat tail, made out of plates bended in one direction, has been added. This modification also included removing the "catwalks".

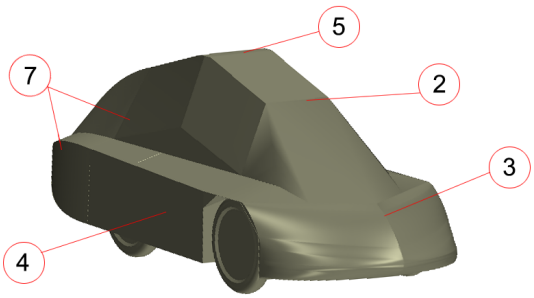

(a) *Final design.*

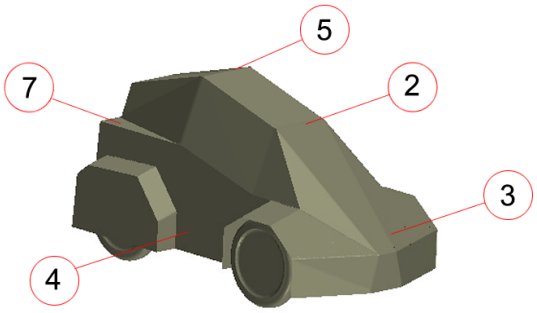

(b) *Original design.*

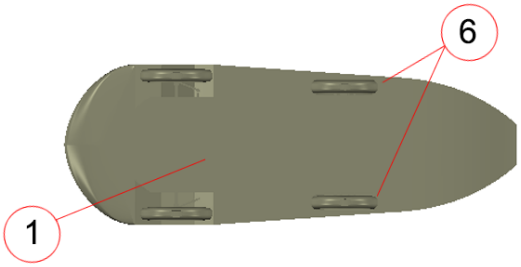

(c) *Undercarriage of the final design.*

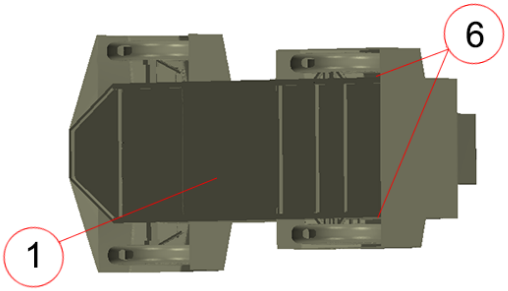

(d) *Undercarriage of the original design. Note that the car is slightly tilted.*

Figure 6.3: *The numbers point to the changes made to the final design compared to the original design. Each change is described in the numbered list in the text above.*

The inner dimensions of the car have not been reduced with the final design, except from the area of the "catwalks". The removal of the "catwalks" resulted in a slight reduction of the inner dimensions. This change is indicated by arrow 7 in figure 6.3b.

6.2 Analysis

A large part of the design process was to design the car to make the flow stay attached as long as possible. In figure 6.4 the isosurfaces of $C_{p,tot} = 0$ are shown to demonstrate how the separation of the flow has changed from the original to the final design. In the front part a clear difference can be seen regarding separation occurring around the front wheel fenders and the A-pillars (see arrow 1 and 2 in figure 6.4a and 6.4b). Next to the front wheels there are still some wakes due to the opening in the wheel arches, although they are the only large separation left throughout the car body. On the top of the car the rounded edges (see arrow 3 in figure 6.4c and 6.4d) contributed to a reduction of separated flow at this point, with only a minor separation remaining. In figure 6.4c the wake behind the boat tail is not shown by the isosurface, although there is still a small wake which can be seen in figure 6.5 and 6.6.

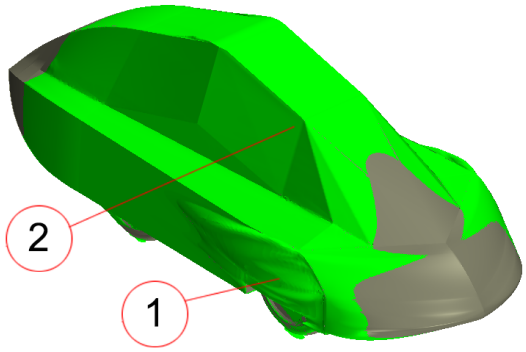

(a) *Final design, front and side view.*

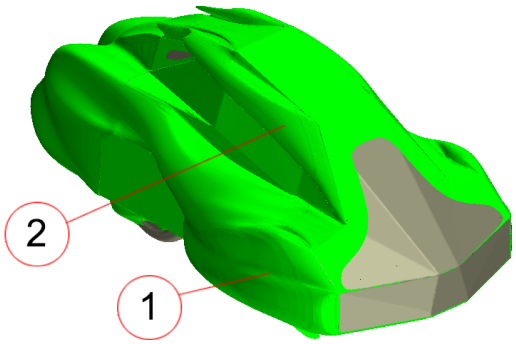

(b) *Original design, front and side view.*

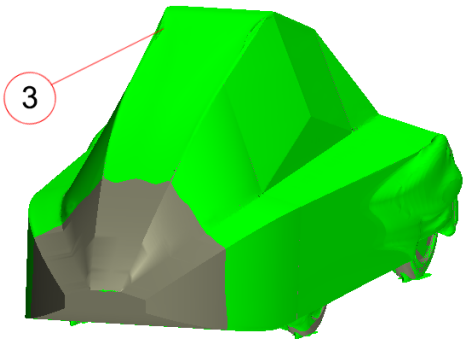

(c) *Final design, back and side view.*

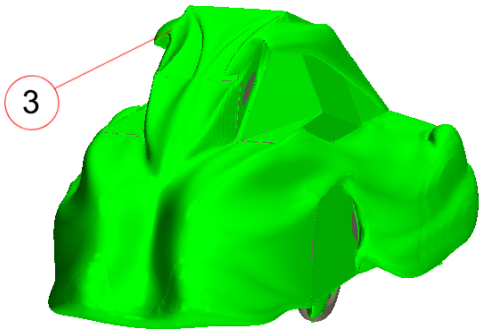

(d) *Original design, back and side view.*

Figure 6.4: *Isosurface of $C_{p,tot} = 0$ of the final and the original design. The numbers illustrate where the changes of the behavior of the flow have occurred.*

The velocity distribution seen from above in figure 6.5 shows differences between the two designs. First of all, an obvious improvement is the wake reduction behind the car, as was mentioned above. This can also be seen in figure 6.6, where the car is seen from the side. Also, a big difference occurs in the region between the front and rear wheels. In the original design the flow recirculates and the velocity drops which indicates losses in the flow. In the final design this space is covered up which eliminates the mentioned problems and makes the flow stay attached along the side of the car. In front of the front wheels (circled in figure 6.5) the end angle was sharpened which makes the wake around the wheels smaller in the final design.

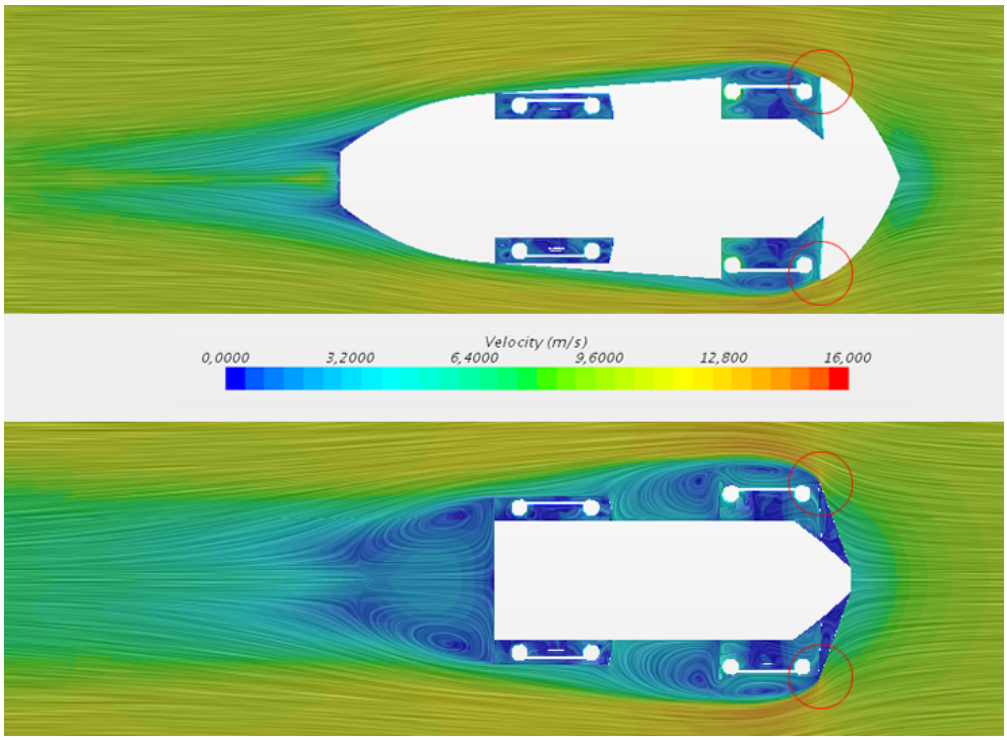

Figure 6.5: *Velocity distribution of the final design (above) and original design (below) seen from above. The velocity is shown in a plane that is located 0.35 m above the ground. The circles indicate where the end angle has been sharpened.*

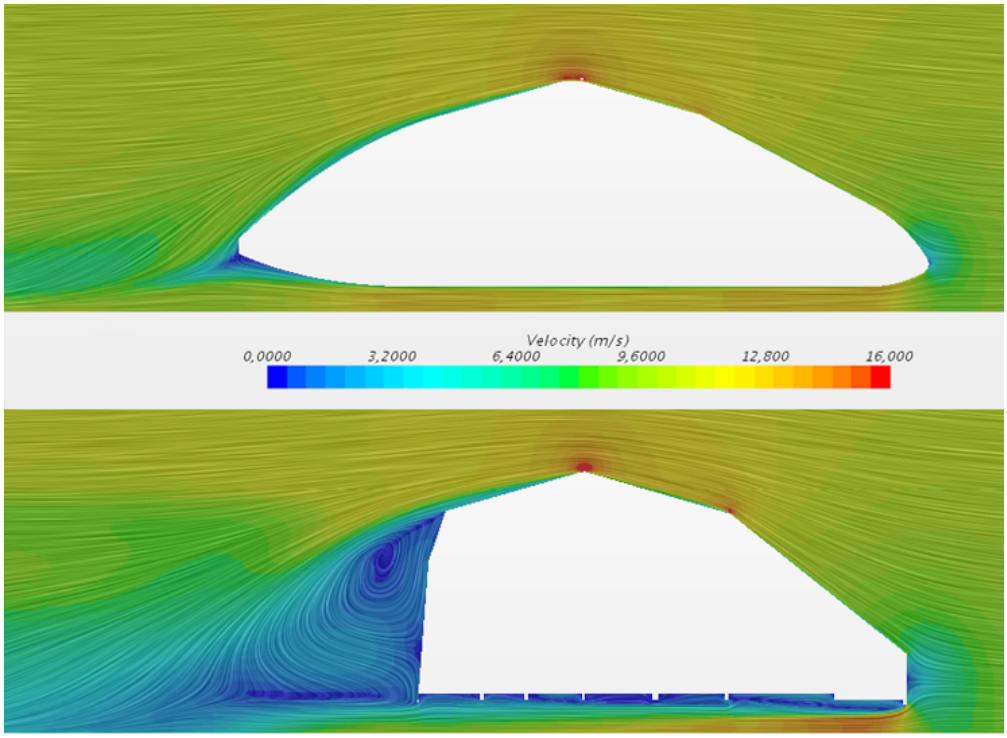

Figure 6.6: *Velocity distribution of the final design (above) and original design (below) seen from the right side.*

In figure 6.7 a comparison of C_p at the front of the car is shown. Due to the nose shaped front in the final design the stagnation zone was reduced.

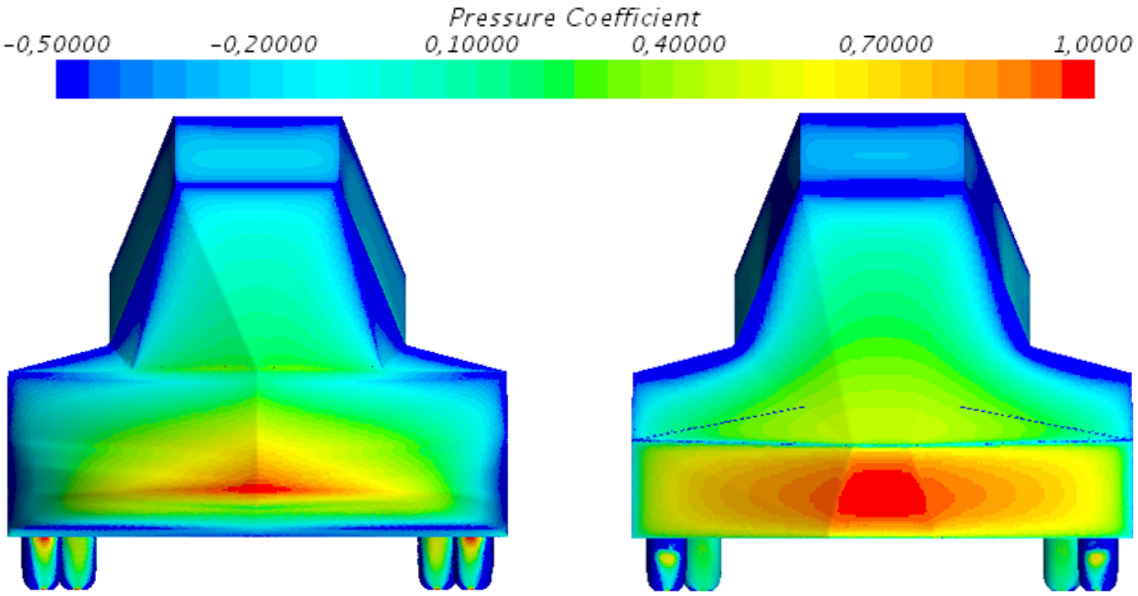

(a) Final design. **(b)** Original design.

Figure 6.7: *Comparison of C_p at the front of the car.*

In figure 6.8 the pressure coefficient is shown on the rear part of the car. In the final design the pressure at the back of the car has increased which implies that the pressure difference between the front and the back is reduced from the original design. This leads to a reduced drag force.

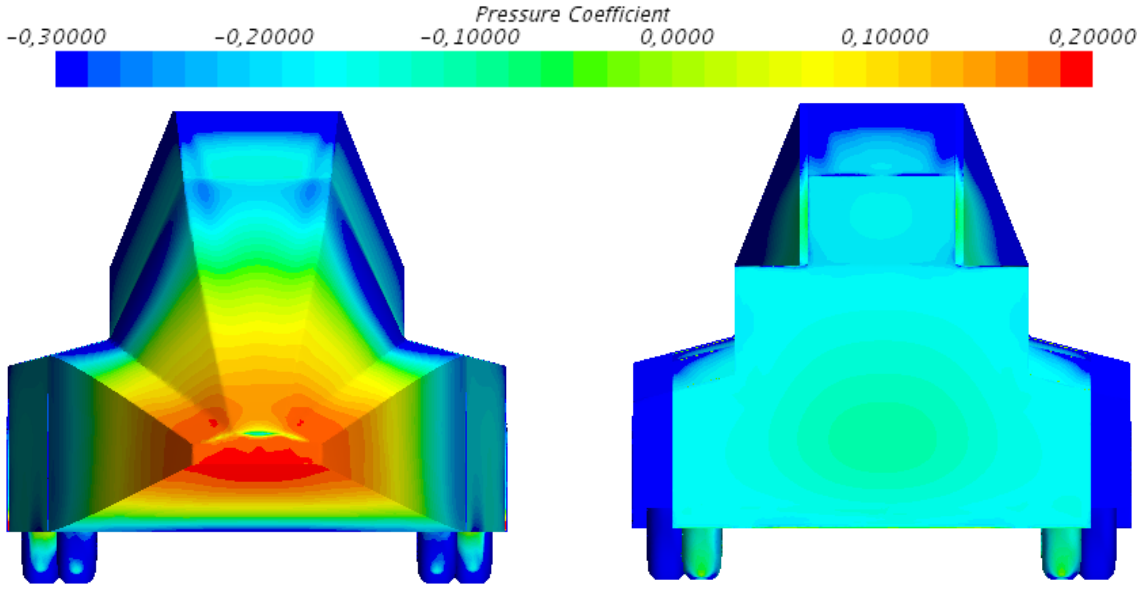

(a) Final design. **(b)** Original design.

Figure 6.8: *Comparison of C_p at the rear of the car.*

The difference in the drag coefficient of the final and original design can be illustrated in figure 6.9. Here the accumulated drag coefficient is plotted over the length of the vehicle.

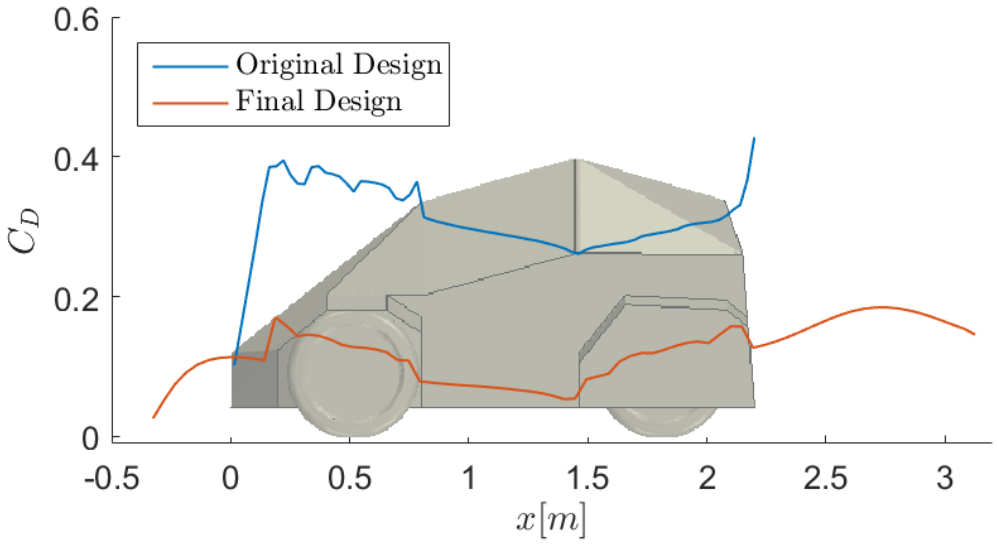

Figure 6.9: *Accumulated drag coefficient, C_D, plotted versus the length of the car, x, for the final and original design.*

In order to know what the improvement of C_D could mean for Smarter in the Shell Eco-marathon competition, the travelled distance can be computed by using theory from section 2.3. By using this theory along with the energy content of one litre petrol (34.9 MJ), the efficiency of the powertrain, last years traveling distance (135 km) and the drag coefficient obtained in the study of the original design, the rolling resistance can be calculated. Unfortunately, the efficiency of the powertrain of Smarter is not known. To be able to make an estimation of the effect that the drag reduction has on the traveling distance an assumption was required regarding powertrain efficiency. It is assumed that Smarter has a powertrain efficiency of 30%. This assumption is based on a typical value for the efficiency of a combustion engine running on the optimal speed, which is around 34% [19].

The rolling resistance F_R was calculated to 47 N for a velocity of 40 km/h. With this result the same equations can be used, together with the drag coefficient of the final design, to calculate the traveling distance. If the only change is the design of the car, this results in a traveling distance of 182 km for the final design, which is an increase of 35% in comparison with the result of 2015.

7
Discussion

This chapter includes a discussion about the used methods and the obtained results. The discussion is based on reflections, criticism and comparisons.

7.1 Comments on Methods

In order to do a CFD analysis, several simplifications and assumptions had to be made which led to an uncertainty of the correctness of the results. First of all, clean-up operations in the pre-processing stage were required to make the surfaces appropriate for CFD simulations. The clean-up process of the original design implied simplifications as closing the opening in the undercarriage and removing several smaller surfaces around the wheels and wheel suspensions among others. The other configurations did not have the opening in the undercarriage and the small surfaces around the wheels, meaning that there was no need for these simplifications. However, the other configurations still have the simplifications regarding the wheels and the wheel suspensions.

Moving forward to the processing, this part also involved various simplifications. For instance, the velocity of the flow was set to be constant, transient effects were disregarded and the flow encountering the car was set to one directional which excluded the influence of side winds. The flow was also assumed to be at steady state, which is not true since for example turbulence varies with time. The simplifications mentioned probably made the result differ from reality. However, many of them are common in this kind of analysis, meaning that the result can be compared to other results from similar CFD studies. Nevertheless, it is important to mention these simplifications since the resulting flow is not the same in reality, which should be considered when analysing the results.

Various assumptions within the theory of fluid dynamics were also made regarding the properties of the fluid. One of the assumptions is that air is treated as a newtonian fluid, something that is needed for applying Navier-Stokes equations. However, this is an established simplification and is not considered to contribute to a significant error. Another assumption used as a physical model in the simulations is that air is an incompressible fluid. Even though this is just an assumption, it is a common approximation used for velocities below 114 m/s. Since the velocity of Smarter is set to 40 km/h, around 11 m/s, this assumption is considered valid in this project. Nevertheless, the assumption of incompressible flow may not be valid

in other studies where higher speed is studied.

The mesh dependency study was performed only on the original design. This study led to the conclusion that a base size of 8 mm would capture the flow behaviour of interest on the original design without being neither too fine nor too coarse. Even though this base size was chosen with some margin, there is no guarantee that the mesh was sufficient for the simulations that followed.

CFD, which is the method used in this project, is an established method in the study of vehicle aerodynamics. Another method widely used within this field is wind tunnel testing. These two methods are often combined by doing CFD simulations followed by tests in a wind tunnel. Even though wind tunnels are used for physical testing, the conditions are not the same as in a real situation and will therefore not give results that fully correspond to reality. The wind tunnel testing has different sources of error than CFD, which means that comparing the results from the two different methods could validate the credibility of the results. Hence, the reliability of the results of this project could have been validated with physical testing in a wind tunnel.

The real car is impossible to build exactly like the CAD model, especially since there are limitations considering the manufacturing. This means that the real car will have flaws that do not exist in the CAD model. For example, when two plates meet there could be a small opening, which affects the flow. Errors like this are probably greater and more frequent for Smarter compared to common cars, due to cost and manufacturing limitations. Furthermore, the abrasiveness in the material that Smarter is built of is not included in the geometry of the CAD model, meaning that the friction on the surface probably is smaller in the simulation compared to the reality.

Another way to achieve the purpose of this project could be to design a completely new car, without starting from the original design. This implies that the new car is designed from scratch and nothing from the original geometry is kept. By having this approach the design would probably look completely different. Furthermore, this means that the inside of the car could be optimized in order to get the frontal area as small as possible. In this project, the inner geometry of the car was not known which implied that decreasing the inner dimensions was restricted.

7.2 Comments on Results

This section presents a discussion about the results from the final design, as well as for other configurations. Some suggestions for further improvements are also included.

7.2.1 Final Design

The original design of Smarter had a C_D of 0.427 and the initial goal was to decrease this value by 10%. To get an apprehension of which values of C_D that are typical

for cars in general, some values of the drag coefficient for other cars are presented in table 2.1 in section 2.2.3. Getting close to these values did not seem possible in the beginning. Nevertheless, the original goal of a decrease by 10% was reached already after standard 1. This configuration resulted in a C_D of 0.379, which is approximately 11% lower than the original. At that point, the aim throughout the rest of the project became to decrease the drag coefficient as much as possible. The final design resulted in a C_D of 0.146, which is far better than imagined in the beginning of the project and close to DTU Dynamo, which is one of the best cars participating in the UrbanConcept class, with a C_D of 0.14.

The car Volkswagen XL1 is considered to be one of the best on the market regarding aerodynamics having a C_D of 0.19, which is presented in table 2.1 in section 2.2.3, yet the final design has a lower C_D. The reason that such a low value could be achieved in this project is the absence of complex components on Smarter compared to production cars. Regarding this type of cars, there is both an interior and an exterior flow. This includes the flow through the engine compartment, ventilation and cooling systems which can not be avoided and increases the total drag.

Considering the lift coefficient, the value of the original design was -0.050 and the value of the final design was -0.039. The lift force of the original and final design can be computed using equation 2.17 in section 2.1.10, resulting in -3.7 N and -2.9 N respectively. The difference between these two are very small. This corresponds to the theory about lift force that can be found in section 2.2.2, stating that the lift force has very small effect on the vehicle for velocities below 100 km/h. This is also the reason why the value was not presented for the other designs.

In order to fulfill the purpose of this thesis, the restrictions of manufacturing the car had to be taken into account. Even though the final design contains more complex geometries than the original design, it should still be possible for the Smarter team to implement. Most of the rounded edges and parts of the car can be built using plates that are bent around one axis. More complex geometries, such as the nose at the front, could be built in e.g. styrofoam, which is easy to form and has a low weight. The original chassis and interior parts can probably still be used, making the implementation of the new design easier and more cost efficient.

In the analysis of the traveling distance a powertrain efficiency of 30% was used, which was based on the efficiency of a combustion engine. Since the powertrain of Smarter consists of other components in addition to a combustion engine, including an electric motor, the real efficiency is probably lower than 30%. This would result in an even longer traveling distance. Although a powertrain efficiency of 30% was used in the calculations, the obtained result considering the difference in traveling distance between the original and the final design, which was 47 km, indicates that an implementation of the final design would be beneficial.

7.2.2 Other Configurations

Even though the final design was the best design presented during this project with respect to aerodynamics, it is not the easiest for the Smarter team to implement. Therefore, some of the other configurations are to be discussed as well in order to weigh simplicity in implementation against losses in drag.

Instead of choosing the long nose shaped front as in the final design, the short nose shaped front could be used. This change does not result in as good C_D as the long nose shape, but the implementation is much easier. Instead of reshaping the whole front, the original front can be used with an attached nose part. This part can be made out of e.g. styrofoam. This design would however probably not remove the vortices around the A-pillars like the frontal shape used in the final design does. Nevertheless, the rounded A-pillars can be used together with the short nose to prevent the flow from separating at the sharp angles at the A-pillars. This is a bit trickier for the Smarter team to implement though. The front part of the original design needs reshaping in order to round the A-pillars, but the main parts of the front can be maintained.

Considering the rear of the car, the configurations with boat tails had by far the lowest drag coefficients. If the boat tail in the final design is too complex to manufacture, an edgy boat tail could be used instead. This could be built of flat plates and will still give a satisfying C_D. Another, even easier approach, is to use the cavity design. This solution probably weighs less compared to the boat tails, but the value of C_D is not as good. The cavity is shorter than the boat tails, which probably makes the car more manageable. If an extension at the rear of the car is not desirable, modifications with the rounded top, in section 5.4.3, and removed plateaus at the rear, in section 5.5, could be implemented in order to make the flow stay attached longer and decrease the wake.

7.2.3 Further Improvements

One of the main limitations of a design process is time. How much improvement in design that is achieved in the end of the project is mainly a matter of how long the project could be run. Even though the purpose of this thesis was achieved, the final design of this project could be subject to further improvement and analysis.

Another significant restriction was the possibility to build the car at Chalmers in order to decrease the costs for materials and material processing. This in turn limited the car to being designed with a combination of flat plates and plates that are bent around one axis. With this in consideration, not all edges from the original design could be removed without increasing the difficulty of manufacturing the car, especially in the rear and middle parts. For instance, without these restrictions the flow separation around the back, prior to attaching the boat tail in the final design, could have been prevented in other ways than the ones used in this thesis. This gives the possibility of completely different designs that might make the car tidier and more limber. As an example, the roof and the rear parts can be rounded in

multiple directions, thus smoothing out the flow around the car.

Regarding the final design, there are still some problematic areas around the vehicle which can be improved. One of them is the regions near the front wheels which still give rise to big wakes. This could be prevented by covering the wheels with flat plates, in the same way as for the rear wheels. The difference here is that the front wheels need more space in order to turn, meaning that this solution is not possible without broadening the whole car. This would increase the frontal area which in turn would increase the drag force. Nevertheless, this is a valid configuration that might result in a decreased C_D. Another way of covering the front wheels would be to use concave plates and broaden the car at just this point. This is easier than broadening the whole car, but it still increases the frontal area and creates a more complex geometry. A critical aspect of doing this is that it can cause the flow to separate in an uncontrolled way, similar to the rounded front wheel fenders.

The height of the final design has been slightly reduced, from 1188 mm in the original design to 1175 mm in the final. Shell Eco-marathon regulations states that the car's height can be as low as 1000 mm. A further lowering of the height would be preferable since this would decrease the frontal area and hence the drag force. This has not been considered in this design process due to the delimitations of the project, where it is stated that the chassis should not be modified. However, if the chassis was to be altered, the regulations of the competition regarding the inside of the cockpit must be taken into consideration when lowering the height.

Furthermore, an iterative approach can be done on every change made throughout the project to achieve optimal angles, radiuses, shapes, etc. In the design process many geometries were arbitrary chosen to get a rough estimation of their effect on drag reduction, and some of them might need a refinement.

8

Conclusion

The main conclusions from this project are:

- The simplifications that were made during the clean-up process and in the processing phase have decreased the credibility of the results.
- Even if the results from the CFD simulations differ from reality the fact that the drag has been heavily reduced is predominant.
- Even small changes in geometry can have large impact on drag force, standard 1 is a good example.
- When the flow is to separate, it should be done abruptly. The rounded front wheel fenders configuration demonstrates the consequences of an uncontrolled flow separation.
- The lift force is slightly changed in conjunction with as low velocities as the velocity of Smarter.
- The drag coefficient was much more reduced than expected in the beginning of this project.
- Further improvements could be achieved given the time.
- The obtained results indicate that an implementation of the final design would be beneficial.

Bibliography

[1] Shell Eco-marathon. About Shell Eco-marathon. http://www.shell.com/energy-and-innovation/shell-ecomarathon/about.html. Accessed: 2016-03-07.

[2] Shell Eco-marathon. Shell Eco-marathon 2016 Official Rules. http://www.shell.com/energy-and-innovation/shell-ecomarathon/for-participants/rules-and-competition-overview.html. Accessed: 2016-03-07.

[3] Chalmers Eco Smarter. About Smarter (2015). http://www.chalmersecosmarter.com/. Accessed: 2016-05-02.

[4] Frank M White. *Fluid Mechanics*. McGraw-Hill, 2011.

[5] Sundén. *Kompendium i värmeöverföring*. 1998.

[6] T.-H. Shih et al. A New k-ϵ Eddy Viscosity Model for High Reynold's Number Turbulent Flows-Model Development and Validation. Technical report, Institute for Computational Mechanics in Propulsion and Center for Modeling of Turbulence and Transition, Lewis Research Center, Cleveland, Ohio, August 1994.

[7] Alf-Erik Almstedt. Fluid mechanics, 2015. Lecture Notes, Chalmers University of Technology.

[8] Walter Frei. Which Turbulence Model Should I Choose for My CFD Application? https://www.comsol.com/blogs/which-turbulence-model-should-choose-cfd-application/. Accessed: 2016-05-03.

[9] Wolf-Heinrich Hucho. *Aerodynamics of Road Vehicles, From Fluid Mechanics to Vehicle Engineering*. Butterworth & Co., 1987.

[10] Lennert Sterken. *Analysis of the Unsteady Flow Field of a Passenger Vehicle*. Department of Applied Mechanics, Chalmers University of Technology, 2015.

[11] Highsnobiety. Volkswagen XL1 – The Most Aerodynamic Production Car Ever. http://www.highsnobiety.com/2013/02/21/volkswagen-xl1-the-most-aerodynamic-production-car-ever/. Accessed: 2016-05-17.

[12] Lisbeth Lassen. DTU Dynamo: Aerodynamik. http://ecocar.dk/. Accessed: 2016-05-12.

[13] Volkswagen. Concepts and Future Cars: XL1. http://www.volkswagen.co.uk/about-us/futures/xl1. Accessed: 2016-05-12.

[14] Cars.com. C2013 Volvo S60. http://www.cars.com/volvo/s60/2013/specifications/. Accessed: 2016-05-16.

[15] Don Sherman. Drag Queens. https://www.teslamotors.com/sites/default/files/blog_attachments/the-slipperiest-car-on-the-road.pdf. Accessed: 2016-05-16.
[16] R. Barnard. *Road Vehicle Aerodynamic Design*. Mechaero Publishing, Cornwall, Great Britain, 2001.
[17] Eric W Weisstein. Finite volume method. http://mathworld.wolfram.com/FiniteVolumeMethod.html. From MathWorld–A Wolfram Web Resource. Accessed: 2016-04-18.
[18] Simone Sebben. Short introduction to CFD. 2016.
[19] Mehrdad Ehsani. *Modern Electric, Hybrid Electric, and Fuel Cell Vehicles-Fundamentals, Theory, and Design*. CRC Press LLC, Boca Raton, 2005c.